

Multiple-distribution-function lattice Boltzmann method for convection-diffusion-system-based incompressible Navier-Stokes equations

Zhenhua Chai ^{1,2,*}, Baochang Shi ^{1,2,†} and Chengjie Zhan ¹

¹*School of Mathematics and Statistics, Huazhong University of Science and Technology, Wuhan 430074, China*

²*Hubei Key Laboratory of Engineering Modeling and Scientific Computing, Huazhong University of Science and Technology, Wuhan 430074, China*



(Received 6 January 2022; accepted 13 October 2022; published 9 November 2022)

In this paper, a multiple-distribution-function lattice Boltzmann method (MDF-LBM) with a multiple-relaxation-time model is proposed for incompressible Navier-Stokes equations which are considered as coupled convection-diffusion equations. Through direct Taylor expansion analysis, we show that the Navier-Stokes equations can be recovered correctly from the present MDF-LBM, and additionally, it is also found that the velocity and pressure can be directly computed through the zero and first-order moments of the distribution function. Then in the framework of the present MDF-LBM, we develop a locally computational scheme for the velocity gradient in which the first-order moment of the nonequilibrium distribution is used; this scheme is also extended to calculate the velocity divergence, strain rate tensor, shear stress, and vorticity. Finally, we also conduct some simulations to test the MDF-LBM and find that the numerical results not only agree with some available analytical and numerical solutions but also have a second-order convergence rate in space.

DOI: [10.1103/PhysRevE.106.055305](https://doi.org/10.1103/PhysRevE.106.055305)

I. INTRODUCTION

In the past three decades, the lattice Boltzmann method (LBM), as a discrete numerical approach to the Boltzmann equation, has had great success in the study of complex fluid flows (for more details, see the review articles in Refs. [1–5] and monographs in [6–10]), including multicomponent and multiphase flows [2,5,8–10], thermal flows [7,8], turbulent flows [1,2,6,7], particle suspensions [3], microfluidics [3,8], and flows in porous media [2,4,7], to name but a few.

Recently, a vectorial lattice Boltzmann method (VLBM) based on the vectorial kinetic model, e.g., the general Bhatnagar-Gross-Krook (BGK) model [11–13] was also developed for shallow water equations [14] and incompressible Navier-Stokes equations (NSEs) [15–17]. Actually, for isothermal and incompressible fluid flows in which the density is assumed to be constant, the NSEs can be viewed as a convection-diffusion system consisting of $(d + 1)$ equations in d -dimensional space and are called convection-diffusion-system-based NSEs here [see the following Eq. (2)]. The main idea of the VLBM is to construct a single evolution equation of the distribution function for each convection-diffusion equation (CDE). Like the double-distribution-function LBM for thermal fluid flows [18–20], the VLBM can also be considered a special multiple-distribution-function lattice Boltzmann method (MDF-LBM), which is used in the present work.

Compared to the popular scalar or single-distribution-function (SDF) LBM for the NSEs, the MDF-LBM

(or VLBM) for convection-diffusion-system-based NSEs has some distinct features. The first is that one can use fewer discrete velocities to construct the MDF-LBM. For instance, if we consider two-dimensional problems, the LBM with the D2Q4 or D2Q5 (four or five discrete velocities in two-dimensional space) lattice model is enough for the CDEs [21], while in the SDF-LBM for the NSEs, the D2Q9 lattice model is usually adopted since the high-order isotropy of the discrete velocities is needed [22]. The second is that in the MDF-LBM for convection-diffusion-system-based NSEs, it is more flexible and much easier to construct the equilibrium distribution function such that the CDEs can be recovered correctly. The third is that in the MDF-LBM for convection-diffusion-system-based NSEs, some physical variables, for example, the velocity gradient, the velocity divergence, the strain rate tensor, the shear stress, and the vorticity, can be calculated locally through the first-order moments of the nonequilibrium distribution function (see Sec. III for details), while in the commonly used SDF-LBM for NSEs, the second-order moments of the nonequilibrium distribution function are needed to compute the strain rate tensor and shear stress [23–26], and what is more, it seems more difficult to directly develop the local scheme for the velocity gradient or vorticity [27].

In this work, inspired by the VLBM for the NSEs [15–17], we develop a MDF-LBM for the convection-diffusion-system-based incompressible NSEs. However, there are four main differences from previous works [15–17]: (1) We focus on the MDF-LBM for incompressible NSEs, and the compressible effect in Refs. [15–17] is neglected. (2) We propose a special formula with the first-order moment of the distribution function for the pressure, which is not only different from those considered in the previous works [15–17] but also stricter theoretically. (3) The formula for the pressure is

*hustczh@hust.edu.cn

†Corresponding author: shibc@hust.edu.cn

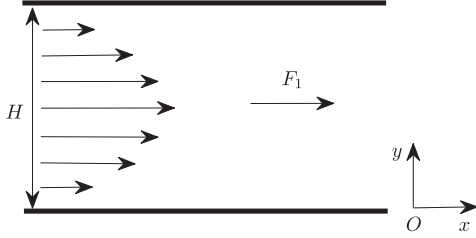


FIG. 1. The schematic of the Poiseuille flow.

consistent with the continuity equation, and thus, the lattice Boltzmann model for the continuity equation can be omitted. (4) We develop some local schemes for the velocity gradient, velocity divergence, strain rate tensor, shear stress, and vorticity, which have not been presented or discussed in the previous works [15–17].

The rest of this paper is organized as follows. In Sec. II, we develop a MDF-LBM for convection-diffusion-system-based incompressible NSEs, and then the direct Taylor expansion of the present MDF-LBM is carried out in Sec. III. In Sec. IV, we present some numerical results and discussion, and finally, some conclusions are given in Sec. V.

II. MULTIPLE-DISTRIBUTION-FUNCTION LATTICE BOLTZMANN METHOD FOR INCOMPRESSIBLE NAVIER-STOKES EQUATIONS

In this section, we first write the incompressible NSEs as a coupled convection-diffusion system and then present a MDF-LBM for the convection-diffusion-system-based incompressible NSEs.

A. The convection-diffusion-system-based incompressible Navier-Stokes equations

For incompressible fluid flows in which the density ρ is assumed to be a positive constant ρ_0 , the NSEs can be written as [28,29]

$$\nabla \cdot \mathbf{u} = R, \quad (1a)$$

$$\frac{\partial \mathbf{u}}{\partial t} + \nabla \cdot (\mathbf{u}\mathbf{u}) = -\nabla P + \nabla \cdot (v\nabla \mathbf{u}) + \mathbf{F}, \quad (1b)$$

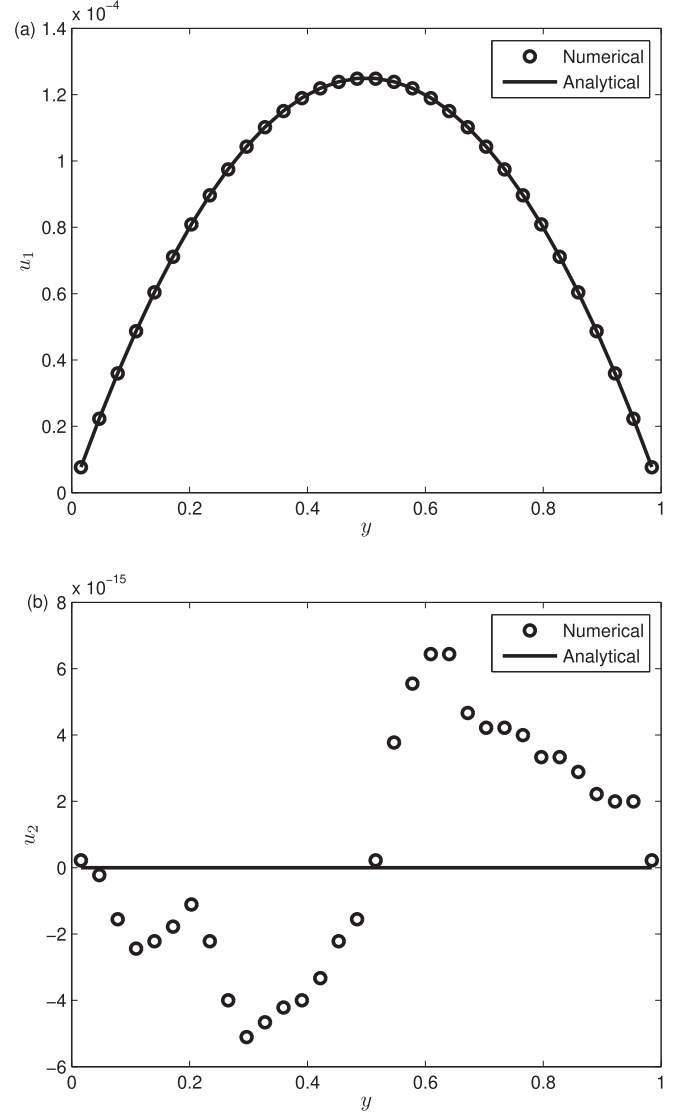
where $\mathbf{u} = (u_\alpha)_{\alpha=1-d}$ is the velocity in d -dimensional space, R is a source term, P is the pressure, v is the kinematic viscosity, and $\mathbf{F} = (F_\alpha)$ is the external force. We would like to point out that the above NSEs can also be reformulated as a coupled convection-diffusion system,

$$\frac{\partial \bar{u}_\alpha}{\partial t} + \nabla \cdot (\bar{u}_\alpha \mathbf{u} + P\mathbf{E}_\alpha) = \nabla \cdot (v\nabla \bar{u}_\alpha) + \bar{F}_\alpha, \quad (2)$$

$$\alpha = 0, 1, \dots, d,$$

where $\bar{\mathbf{u}} = (\bar{u}_\alpha)$, with $\bar{u}_0 = \rho_0$ and $\bar{u}_\alpha = u_\alpha$ ($\alpha = 1-d$); $\bar{\mathbf{F}} = (\bar{F}_\alpha)$, with $\bar{F}_0 = R$ and $\bar{F}_\alpha = F_\alpha$ ($\alpha = 1-d$); $\mathbf{E}_0 = \mathbf{0}$ and \mathbf{E}_α ($\alpha = 1-d$) is the unit vector in d -dimensional space.

It is clear that Eq. (2) is composed of $d+1$ CDEs, and in the following, it is considered to be the convection-diffusion-system-based NSEs. We note that although the incompressible NSEs (1) are equivalent to Eq. (2) mathematically, the latter is just a convection-diffusion system and can be solved more


 FIG. 2. The numerical and analytical solutions of the velocity. (a) u_1 and (b) u_2 .

efficiently with the LBM. Actually, in the LBM for the CDE, only the third-order isotropy of the discrete velocity is needed, which brings more flexibility to the development of the lattice Boltzmann (LB) models; however, in the SDF-LBM for NSEs, the fifth-order isotropy of discrete velocity is required, which gives rise to more limitations in the design of the LB models.

B. The multiple-distribution-function lattice Boltzmann method for the convection-diffusion-system-based Navier-Stokes equations

In the LBM, the LB models can be classified into three basic kinds, i.e., the single-relaxation-time LB (SRT-LB) model or lattice BGK model [22,30], the two-relaxation-time LB (TRT-LB) model [31,32], and the multiple-relaxation-time LB (MRT-LB) model [33,34], and it can also be shown that the SRT-LB model and TRT-LB model are two special cases of the MRT-LB model [35]. In this work, we consider the MRT-LB model for its generality, accuracy, and stability. In terms

TABLE I. A comparison of Galilean invariance between the present MDF-LBM and SDF-LBM.

| | 0 | 0.01 | u_0 0.05 | 0.085 | 0.1 |
|-------------------|--------------------------|-------------------------|-------------------------|-------------------------|-------------------------|
| MDF-LBM | | | | | |
| $E_{L^2}(u_1)$ | 5.9427×10^{-4} | 5.9286×10^{-4} | 5.9971×10^{-4} | 5.9971×10^{-4} | |
| $E_{L^2}(S_{xy})$ | 3.3213×10^{-17} | 1.0027×10^{-6} | 5.0363×10^{-6} | 3.7202×10^{-6} | |
| $E_{L^2}(\omega)$ | 3.3213×10^{-17} | 9.8942×10^{-7} | 5.0145×10^{-6} | 3.7254×10^{-6} | |
| SDF-LBM | | | | | |
| $E_{L^2}(u_1)$ | 5.4478×10^{-4} | 5.4453×10^{-4} | 5.4453×10^{-4} | 5.4453×10^{-4} | 4.922×10^{-4} |
| $E_{L^2}(S_{xy})$ | 1.8386×10^{-3} | 1.8386×10^{-3} | 1.8386×10^{-3} | 1.8386×10^{-3} | 1.8386×10^{-3} |
| $E_{L^2}(\omega)$ | 1.8385×10^{-3} | 1.8385×10^{-3} | 1.8385×10^{-3} | 1.8385×10^{-3} | 1.8385×10^{-3} |

of accuracy, Ginzburg and d'Humières [36] performed an analysis of the bounce-back boundary condition of the LBM for the Poiseuille flow and found that the *numerical* slip on the solid wall can be reduced or eliminated by setting the free parameter(s) in the MRT-LB or TRT-LB model, which can also be used to derive the viscosity-independent permeabilities of the porous media [37,38]. We note that this result has also been extended to the MRT-LB or TRT-LB model coupled with the anti-bounce-back boundary condition for the CDEs [21,39–42], and the diffusion-dependent error can be reduced or removed to give accurate effective diffusivities of porous media [43,44]. In terms of stability, the MRT-LB model can be more stable than the SRT-LB model and the TRT-LB model by adjusting the free parameters properly, as shown in a previous work [45]. In the past years, some different MRT-LB models were developed for the isotropic and anisotropic CDEs [41,46–49]. Recently, Chai and Shi proposed a unified framework for the modeling of the MRT-LB models for the NSEs and nonlinear CDEs [35]. Following this work and with inspiration from the VLBM [14–17], the evolution equation of the MDF-LBM for the convection-diffusion-system-based NSEs (2) can be written as

$$\begin{aligned}
 f_{i,\alpha}(\mathbf{x} + \mathbf{c}_i \delta t, t + \delta t) &= f_{i,\alpha}(\mathbf{x}, t) - \Lambda_{ik} [f_{k,\alpha}(\mathbf{x}, t) - f_{k,\alpha}^{\text{eq}}(\mathbf{x}, t)] \\
 &+ \delta t \left[G_{i,\alpha}(\mathbf{x}, t) + F_{i,\alpha}(\mathbf{x}, t) + \frac{\delta t}{2} \bar{D}_i F_{i,\alpha}(\mathbf{x}, t) \right], \quad (3)
 \end{aligned}$$

where $f_{i,\alpha}(\mathbf{x}, t)$ is the distribution function corresponding to the variable \bar{u}_α at position \mathbf{x} and time t along the discrete velocity \mathbf{c}_i . δt is the time step; $\bar{D}_i = \partial_t + \gamma \mathbf{c}_i \cdot \nabla$, with the parameter $\gamma \in \{0, 1\}$, which can be discretized by some different first-order difference schemes [35]. $\Lambda = (\Lambda_{ik})$ is a $q \times q$ invertible collision matrix, with q representing the number of discrete velocities. As pointed out in a previous work [35], to recover Eq. (2) from the MDF-LBM (3), some appropriate requirements for the collision matrix Λ are needed:

$$\sum_i \mathbf{c}_i \Lambda_{ik} = s_0 \mathbf{e}_k, \quad \sum_i \mathbf{c}_i \Lambda_{ik} = s_1 \mathbf{c}_k, \quad (4)$$

where $\mathbf{e} = (1, 1, \dots, 1) \in R^q$ and s_0 and s_1 are eigenvalues of the collision matrix Λ or the relaxation parameters corresponding to the zero and first-order moments of the distribution function. Here it should be noted that a more general case of Eq. (4) shown in Ref. [35] can also be

considered. $f_{i,\alpha}^{\text{eq}}(\mathbf{x}, t)$ is the equilibrium distribution function, $G_{i,\alpha}(\mathbf{x}, t)$ is the auxiliary distribution function, and $F_{i,\alpha}(\mathbf{x}, t)$ is the distribution function of the source term \bar{F}_α ; to derive the correct macroscopic equation (2), they should be defined

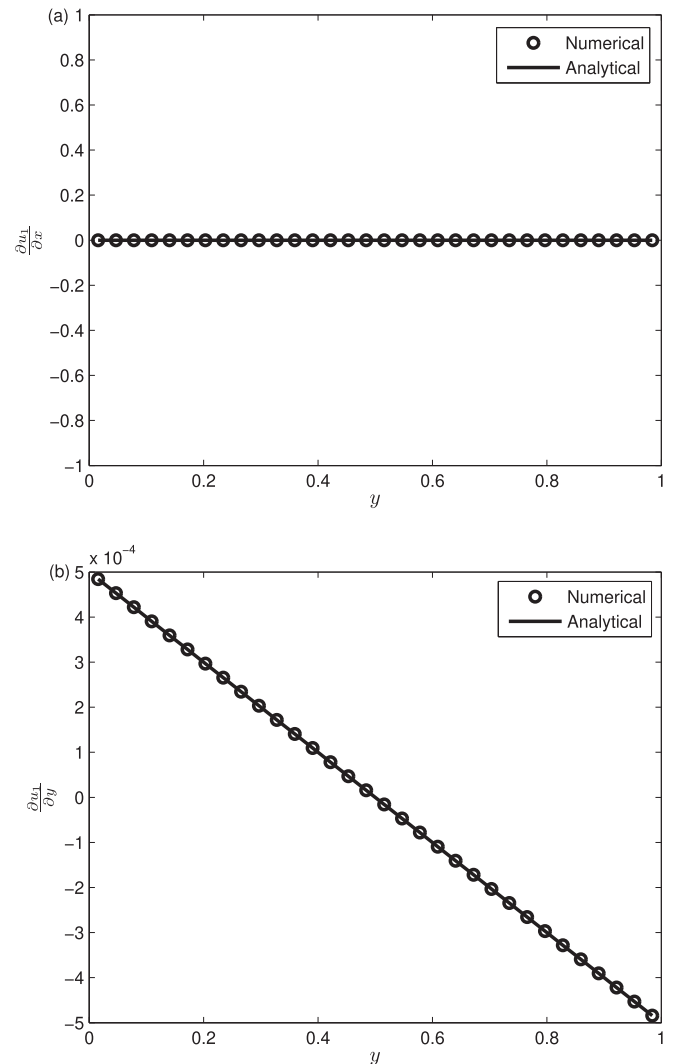


FIG. 3. The numerical and analytical solutions of the velocity gradient. (a) $\partial u_1 / \partial x$ and (b) $\partial u_1 / \partial y$.

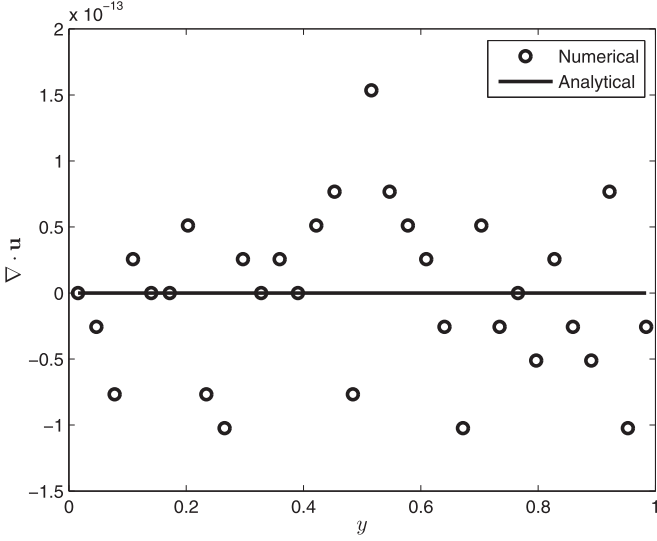


FIG. 4. The numerical and analytical solutions of the velocity divergence.

as [35,50]

$$f_{i,\alpha}^{\text{eq}} = \omega_i \left[\bar{u}_\alpha + \frac{\mathbf{c}_i \cdot (\bar{u}_\alpha \mathbf{u} + P \mathbf{E}_\alpha)}{\eta c^2} \right], \quad (5)$$

$$G_{i,\alpha} = \left(1 - \frac{s_1}{2} \right) \omega_i \frac{\mathbf{c}_i \cdot \partial_t (\bar{u}_\alpha \mathbf{u} + P \mathbf{E}_\alpha)}{\eta c^2}, \quad (6)$$

$$F_{i,\alpha} = \omega_i \bar{F}_\alpha, \quad (7)$$

where the simple linear equilibrium distribution function (5) with respect to the discrete velocity is considered. ω_i is the weight coefficient. η is a scale factor related to viscosity, and $c = \delta x / \delta t$ is the lattice speed, with δx being the lattice spacing. In the $DdQq$ (q discrete velocities in d -dimensional space) lattice model, the discrete velocity \mathbf{c}_i , the weight coefficient ω_i , and the scale factor η should satisfy the following relations:

$$\sum_i \omega_i = 1, \quad (8a)$$

$$\sum_i \omega_i \mathbf{c}_i = \mathbf{0}, \quad (8b)$$

$$\sum_i \omega_i \mathbf{c}_i \mathbf{c}_i = \eta c^2 \mathbf{I}, \quad (8c)$$

where \mathbf{I} is the unit matrix. Here we list some special cases that have been widely used in the LBM.

For the D1Q2 lattice model,

$$\mathbf{c}_i = (1, -1)c, \quad (9a)$$

$$\omega_1 = \omega_2 = \frac{1}{2}, \quad (9b)$$

$$\eta = 1. \quad (9c)$$

For the D1Q3 lattice model,

$$\mathbf{c}_i = (0, 1, -1)c, \quad (10a)$$

$$\omega_0 = \frac{2}{3}, \quad \omega_1 = \omega_2 = \frac{1}{6}, \quad (10b)$$

$$\eta = 1/3. \quad (10c)$$

For the D2Q4 lattice model,

$$\mathbf{c}_i = \begin{pmatrix} 1 & 0 & -1 & 0 \\ 0 & 1 & 0 & -1 \end{pmatrix} c, \quad (11a)$$

$$\omega_1 = \omega_2 = \omega_3 = \omega_4 = \frac{1}{4}, \quad (11b)$$

$$\eta = 1/2. \quad (11c)$$

For the D2Q5 lattice model,

$$\mathbf{c}_i = \begin{pmatrix} 0 & 1 & 0 & -1 & 0 \\ 0 & 0 & 1 & 0 & -1 \end{pmatrix} c, \quad (12a)$$

$$\omega_0 = \frac{1}{3}, \quad \omega_1 = \omega_2 = \omega_3 = \omega_4 = \frac{1}{6}, \quad (12b)$$

$$\eta = 1/3. \quad (12c)$$

For the D2Q9 lattice model,

$$\mathbf{c}_i = \begin{pmatrix} 0 & 1 & 0 & -1 & 0 & 1 & -1 & -1 & 1 \\ 0 & 0 & 1 & 0 & -1 & 1 & 1 & -1 & -1 \end{pmatrix} c, \quad (13a)$$

$$\omega_0 = \frac{4}{9}, \quad \omega_{1-4} = \frac{1}{9}, \quad \omega_{5-8} = \frac{1}{36}, \quad (13b)$$

$$\eta = 1/3. \quad (13c)$$

For the D3Q6 lattice model,

$$\mathbf{c}_i = \begin{pmatrix} 1 & -1 & 0 & 0 & 0 & 0 \\ 0 & 0 & 1 & -1 & 0 & 0 \\ 0 & 0 & 0 & 0 & 1 & -1 \end{pmatrix} c, \quad (14a)$$

$$\omega_{1-6} = \frac{1}{6}, \quad (14b)$$

$$\eta = 1/3. \quad (14c)$$

For the D3Q7 lattice model,

$$\mathbf{c}_i = \begin{pmatrix} 0 & 1 & -1 & 0 & 0 & 0 & 0 \\ 0 & 0 & 0 & 1 & -1 & 0 & 0 \\ 0 & 0 & 0 & 0 & 0 & 1 & -1 \end{pmatrix} c, \quad (15a)$$

$$\omega_0 = \frac{1}{4}, \quad \omega_{1-6} = \frac{1}{8}, \quad (15b)$$

$$\eta = 1/4. \quad (15c)$$

For the D3Q15 lattice model,

$$\mathbf{c}_i = \begin{pmatrix} 0 & 1 & -1 & 0 & 0 & 0 & 0 & 1 & 1 & 1 & -1 & -1 & -1 & 1 & -1 \\ 0 & 0 & 0 & 1 & -1 & 0 & 0 & 1 & 1 & -1 & 1 & -1 & 1 & -1 & -1 \\ 0 & 0 & 0 & 0 & 0 & 1 & -1 & 1 & -1 & 1 & 1 & 1 & -1 & -1 & -1 \end{pmatrix} c, \quad (16a)$$

$$\omega_0 = \frac{2}{9}, \quad \omega_{1-6} = \frac{1}{9}, \quad \omega_{7-14} = \frac{1}{72}, \quad (16b)$$

$$\eta = 1/3. \quad (16c)$$

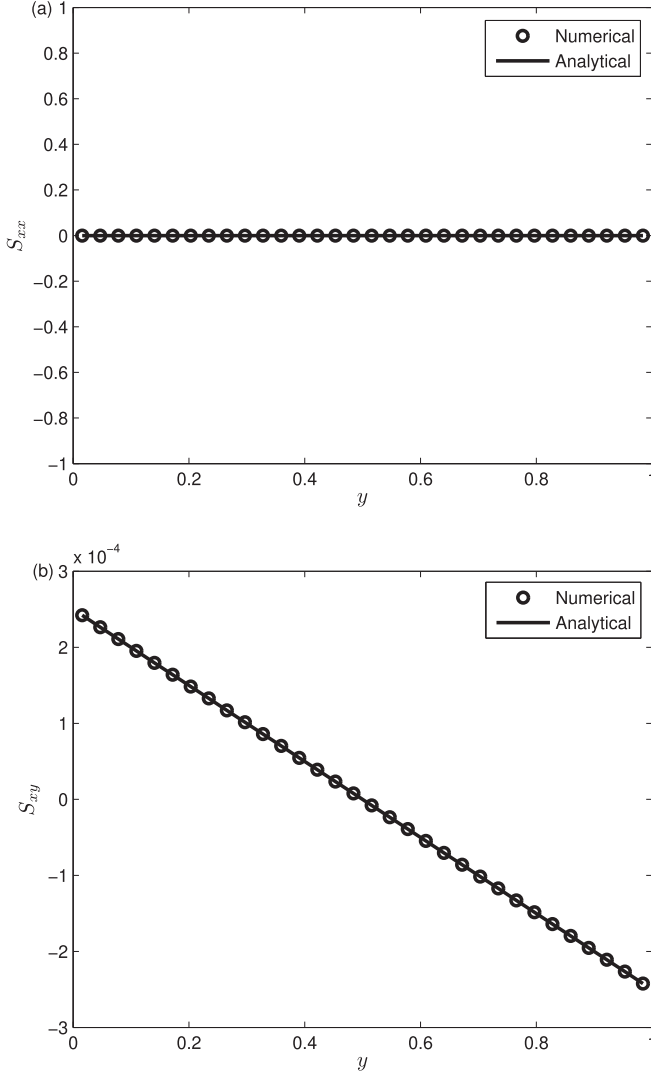


FIG. 5. The numerical and analytical solutions of the strain rate tensor. (a) S_{xx} and (b) S_{xy} .

We would like to point out that different lattice models can be applied for different evolution equations represented by different α . In the MDF-LBM for the convection-diffusion-system-based NSEs, the macroscopic variable \bar{u}_α is computed by

$$\bar{u}_\alpha = \sum_i f_{i,\alpha}. \quad (17)$$

III. THE DIRECT TAYLOR EXPANSION OF THE MULTIPLE-DISTRIBUTION-FUNCTION LATTICE BOLTZMANN METHOD

Historically, there are some asymptotic analysis methods that can be used to derive the macroscopic governing

$$f_{i,\alpha}^{ne} = O(\delta t), \quad (19a)$$

$$\sum_{j=1}^{N-1} \frac{\delta t^j}{j!} D_i^j (f_{i,\alpha}^{eq} + f_{i,\alpha}^{ne}) + \frac{\delta t^N}{N!} D_i^N f_{i,\alpha}^{eq} = -\mathbf{\Lambda}_{ik} f_{k,\alpha}^{ne} + \delta t \left[G_{i,\alpha}(\mathbf{x}, t) + F_{i,\alpha}(\mathbf{x}, t) + \frac{\delta t}{2} \bar{D}_i F_{i,\alpha}(\mathbf{x}, t) \right] + O(\delta t^{N+1}). \quad (19b)$$

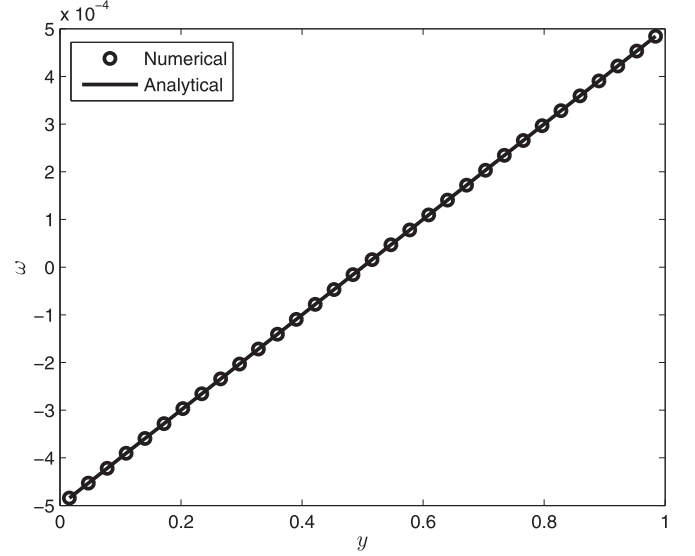


FIG. 6. The numerical and analytical solutions of the vorticity ω .

equation (2) from the MDF-LBM [35], including the Chapman-Enskog analysis [2,51], the Maxwell iteration method [52], the direct Taylor expansion method [53,54], and the recurrence equation method [55]. However, it has been shown that at the second order of expansion parameters, these four analysis methods can give the same macroscopic equations [35]. For this reason, we consider only the direct Taylor expansion method for its simplicity; additionally, compared to the commonly used Chapman-Enskog analysis, this method includes only a single expansion parameter, δt .

A. The direct Taylor expansion

Based on previous works [35,53,54], when the Taylor expansion is applied to Eq. (3), we have

$$\begin{aligned} & \sum_{j=1}^N \frac{\delta t^j}{j!} D_i^j f_{i,\alpha} + O(\delta t^{N+1}) \\ & = -\mathbf{\Lambda}_{ik} (f_{k,\alpha} - f_{k,\alpha}^{eq}) + \delta t \left[G_{i,\alpha}(\mathbf{x}, t) + F_{i,\alpha}(\mathbf{x}, t) \right. \\ & \quad \left. + \frac{\delta t}{2} \bar{D}_i F_{i,\alpha}(\mathbf{x}, t) \right], \quad (18) \end{aligned}$$

where $D_i = \partial_t + \mathbf{c}_i \cdot \nabla$. Introducing $f_{i,\alpha}^{ne} = f_{i,\alpha} - f_{i,\alpha}^{eq}$ and substituting it into the collision term in Eq. (18), we can derive the following equations:

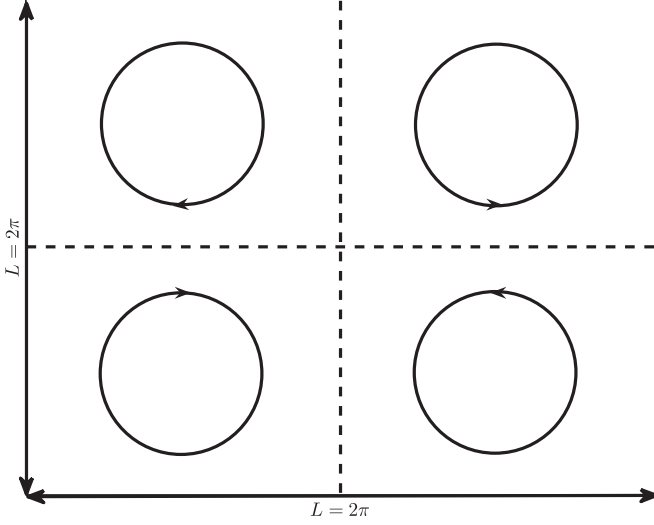


FIG. 7. The schematic of the two-dimensional four-roll mill problem.

Then the equations with the first and second orders of δt can be obtained,

$$D_i f_{i,\alpha}^{\text{eq}} = -\frac{1}{\delta t} \Lambda_{ik} f_{k,\alpha}^{\text{ne}} + (G_{i,\alpha} + F_{i,\alpha}) + O(\delta t), \quad (20a)$$

$$D_i (f_{i,\alpha}^{\text{eq}} + f_{i,\alpha}^{\text{ne}}) + \frac{\delta t}{2} D_i^2 f_{i,\alpha}^{\text{eq}} = -\frac{1}{\delta t} \Lambda_{ik} f_{k,\alpha}^{\text{ne}} + \left(G_{i,\alpha} + F_{i,\alpha} + \frac{\delta t}{2} \bar{D}_i F_{i,\alpha} \right) + O(\delta t^2). \quad (20b)$$

From Eq. (20a), we have

$$\frac{\delta t}{2} D_i^2 f_{i,\alpha}^{\text{eq}} = -\frac{1}{2} D_i \Lambda_{ik} f_{k,\alpha}^{\text{ne}} + \frac{\delta t}{2} D_i (G_{i,\alpha} + F_{i,\alpha}) + O(\delta t^2). \quad (21)$$

Substituting Eq. (21) into Eq. (20b) yields

$$D_i f_{i,\alpha}^{\text{eq}} + D_i \left(\delta_{ik} - \frac{1}{2} \Lambda_{ik} \right) f_{k,\alpha}^{\text{ne}} + \frac{\delta t}{2} D_i (G_{i,\alpha} + F_{i,\alpha}) = -\frac{1}{\delta t} \Lambda_{ik} f_{k,\alpha}^{\text{ne}} + G_{i,\alpha} + F_{i,\alpha} + \frac{\delta t}{2} \bar{D}_i F_{i,\alpha} + O(\delta t^2).$$

Using Eqs. (5), (6), and (7), we can also determine the moments of $f_{i,\alpha}^{\text{eq}}(\mathbf{x}, t)$, $G_{i,\alpha}(\mathbf{x}, t)$, and $F_{i,\alpha}(\mathbf{x}, t)$,

$$\sum_i f_{i,\alpha}^{\text{eq}} = \bar{u}_\alpha, \quad \sum_i \mathbf{c}_i f_{i,\alpha}^{\text{eq}} = \bar{u}_\alpha \mathbf{u} + \mathbf{P} \mathbf{E}_\alpha, \quad (22a)$$

$$\sum_i \mathbf{c}_i \mathbf{c}_i f_{i,\alpha}^{\text{eq}} = \bar{u}_\alpha \eta c^2 \mathbf{I},$$

$$\sum_i G_{i,\alpha} = 0, \quad \sum_i \mathbf{c}_i G_{i,\alpha} = \left(1 - \frac{s_1}{2} \right) \partial_t (\bar{u}_\alpha \mathbf{u} + \mathbf{P} \mathbf{E}_\alpha), \quad (22b)$$

$$\sum_i F_{i,\alpha} = \bar{F}_\alpha, \quad \sum_i \mathbf{c}_i F_{i,\alpha} = \mathbf{0}. \quad (22c)$$

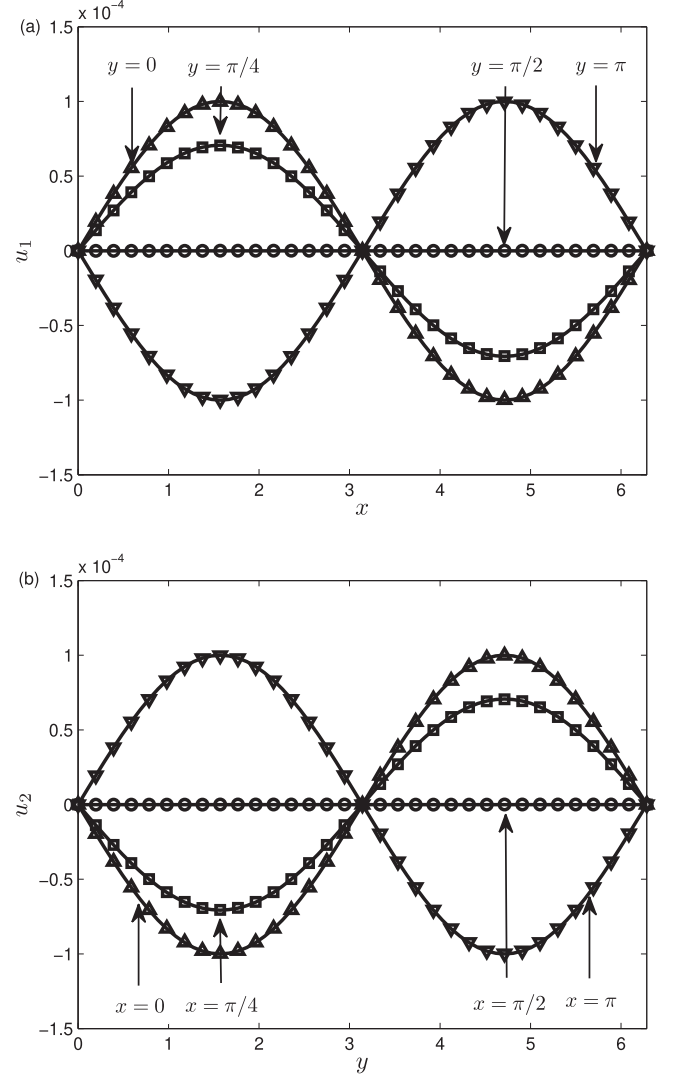


FIG. 8. The numerical and analytical solutions of velocity at different positions. (a) u_1 and (b) u_2 . Solid lines show the analytical solution, and symbols show the numerical solution.

From Eqs. (17) and (22a), we can first obtain

$$\sum_i f_{i,\alpha}^{\text{ne}} = 0. \quad (23)$$

Then with the help of Eq. (4), we can also derive the following equations:

$$\sum_i \mathbf{e}_i \Lambda_{ik} f_{k,\alpha}^{\text{ne}} = s_0 \sum_k \mathbf{e}_k f_{k,\alpha}^{\text{ne}} = \mathbf{0}, \quad (24)$$

$$\sum_i \mathbf{c}_i \Lambda_{ik} f_{k,\alpha}^{\text{ne}} = s_1 \sum_k \mathbf{c}_k f_{k,\alpha}^{\text{ne}}. \quad (25)$$

B. Derivation of the convection-diffusion-system-based Navier-Stokes-equations

We now present some details on how to derive the convection-diffusion-system-based NSEs (2) from MDF-LBM (3). To this end, we conduct a summation of Eq. (22)

TABLE II. The relative errors of the strain rate tensor and vorticity under different computational schemes.

| | Local scheme | Finite-difference scheme |
|-------------------|-------------------------|--------------------------|
| $E_{L^2}(S_{xx})$ | 8.0730×10^{-4} | 3.6808×10^{-3} |
| $E_{L^2}(S_{yy})$ | 8.0730×10^{-4} | 3.6808×10^{-3} |
| $E_{L^2}(\omega)$ | 8.0731×10^{-4} | 3.6808×10^{-3} |

and obtain the following equation:

$$\begin{aligned} \frac{\partial \bar{u}_\alpha}{\partial t} + \nabla \cdot (\bar{u}_\alpha \mathbf{u} + P \mathbf{E}_\alpha) + \nabla \cdot \left[\left(1 - \frac{s_1}{2}\right) \sum_i \mathbf{c}_i f_{i,\alpha}^{ne} \right] \\ + \frac{\delta t}{2} \nabla \cdot \left[\left(1 - \frac{s_1}{2}\right) \partial_t (\bar{u}_\alpha \mathbf{u} + P \mathbf{E}_\alpha) \right] \\ = \bar{F}_\alpha + O(\delta t^2). \end{aligned} \quad (26)$$

Now let us give an evaluation of the term $\sum_i \mathbf{c}_i f_{i,\alpha}^{ne}$. Actually, from Eq. (20a) we have

$$\begin{aligned} \sum_i \mathbf{c}_i f_{i,\alpha}^{ne} &= -\delta t \sum_i \mathbf{c}_i \Lambda_{ik}^{-1} (D_k f_{k,\alpha}^{eq} - G_{k,\alpha} - F_{k,\alpha}) + O(\delta t^2) \\ &= -\frac{\delta t}{s_1} \sum_i \mathbf{c}_i (D_i f_{i,\alpha}^{eq} - G_{i,\alpha} - F_{i,\alpha}) + O(\delta t^2) \\ &= -\frac{\delta t}{2} \partial_t (\bar{u}_\alpha \mathbf{u} + P \mathbf{E}_\alpha) - \frac{\delta t}{s_1} \eta c^2 \nabla \bar{u}_\alpha + O(\delta t^2), \end{aligned} \quad (27)$$

where Eqs. (4) and (22) have been used. Substituting Eq. (27) into Eq. (26) yields

$$\begin{aligned} \frac{\partial \bar{u}_\alpha}{\partial t} + \nabla \cdot (\bar{u}_\alpha \mathbf{u} + P \mathbf{E}_\alpha) = \nabla \cdot \left[\left(\frac{1}{s_1} - \frac{1}{2}\right) \eta c^2 \delta t \nabla \bar{u}_\alpha \right] \\ + \bar{F}_\alpha + O(\delta t^2). \end{aligned} \quad (28)$$

If we neglect the truncation error $O(\delta t^2)$, we can obtain the macroscopic convection-diffusion-system-based NSEs (2) with the following viscosity:

$$\nu = \left(\frac{1}{s_1} - \frac{1}{2}\right) \eta c^2 \delta t. \quad (29)$$

Here we would also like to have a special discussion on how to calculate the pressure P . From Eq. (27) we can get

$$\begin{aligned} \sum_i \mathbf{c}_i f_{i,\alpha}^{ne} &= \sum_i \mathbf{c}_i f_{i,\alpha} - \sum_i \mathbf{c}_i f_{i,\alpha}^{eq} \\ &= \sum_i \mathbf{c}_i f_{i,\alpha} - (\bar{u}_\alpha \mathbf{u}_\alpha + P) \\ &= -\frac{\delta t}{s_1} \eta c^2 \nabla_\alpha \bar{u}_\alpha + O(\delta t^2 + \delta t \text{Ma}^2) \quad (\alpha \neq 0), \end{aligned} \quad (30)$$

where Ma is the Mach number. Neglecting the truncation error term $O(\delta t^2 + \delta t \text{Ma}^2)$ and summing Eq. (30) over α , we can

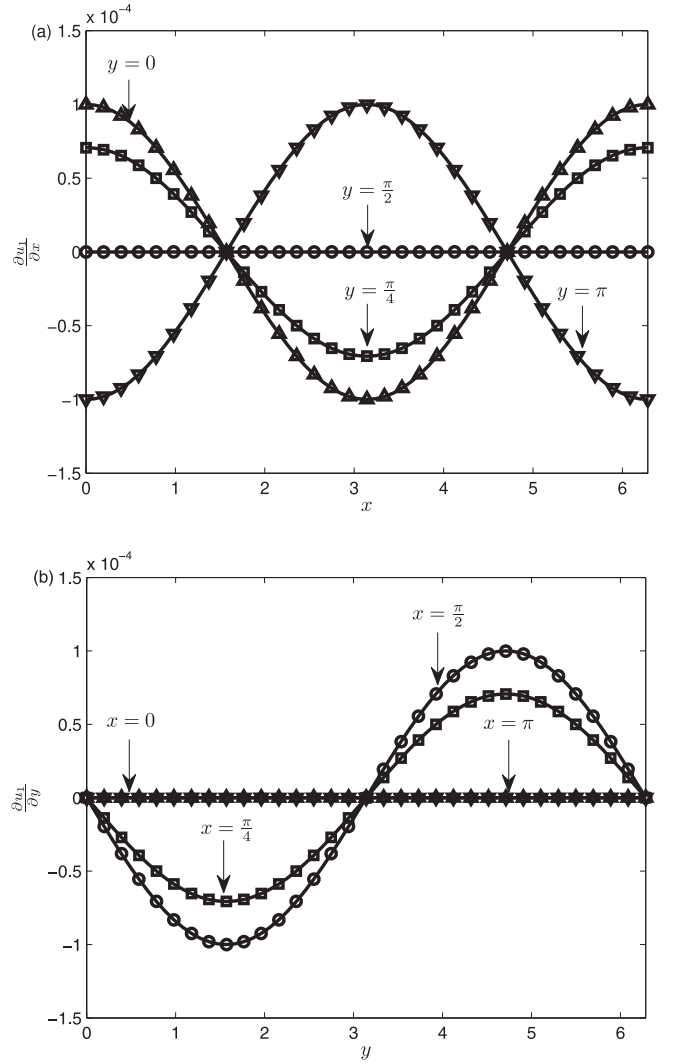


FIG. 9. The numerical and analytical solutions of the velocity gradient at different positions. (a) $\partial u_1/\partial x$ and (b) $\partial u_1/\partial y$. Solid lines show the analytical solution, and symbols show the numerical solution.

derive

$$\sum_{\alpha=1}^d \sum_i \mathbf{c}_i f_{i,\alpha} - (|\mathbf{u}|^2 + dP) = -\frac{\delta t}{s_1} \eta c^2 R, \quad (31)$$

where Eq. (1a) has been used. From Eq. (31) we can give an expression to compute the pressure,

$$P = \frac{1}{d} \left(\sum_{\alpha=1}^d \sum_i \mathbf{c}_i f_{i,\alpha} + \frac{\delta t}{s_1} \eta c^2 R - |\mathbf{u}|^2 \right). \quad (32)$$

In the above procedure, the continuity equation (1a) recovered from the MDF-LBM [see Eq. (28) with $\alpha = 0$] has been used to derive Eq. (32). On the other hand, if Eq. (32) is ensured, the continuity equation (1a) must also be satisfied. In other words, we do not need to consider the continuity equation (1a) in the present MDF-LBM since Eq. (32) is adopted, and the evolution equation (3) with $\alpha = 0$ can be omitted. We also note that the term related to $G_{i,\alpha}$ in Eq. (3) can also be neglected since it is on the order of $O(\delta t \text{Ma}^2)$. In this case,

the evolution equation (3) can be simplified to

$$f_{i,\alpha}(\mathbf{x} + \mathbf{c}_i \delta t, t + \delta t) = f_{i,\alpha}(\mathbf{x}, t) - \Lambda_{ik} [f_{k,\alpha}(\mathbf{x}, t) - f_{k,\alpha}^{\text{eq}}(\mathbf{x}, t)] + \delta t \left[F_{i,\alpha}(\mathbf{x}, t) + \frac{\delta t}{2} \bar{D}_i F_{i,\alpha}(\mathbf{x}, t) \right]. \quad (33)$$

Then we can derive two special schemes [41] from Eq. (33).

Scheme I. $\gamma = 0$. Under this condition, $\bar{D}_i F_{i,\alpha}(\mathbf{x}, t) = \partial_i F_{i,\alpha}(\mathbf{x}, t)$. Considering the Euler method for the time derivative, we have

$$f_{i,\alpha}(\mathbf{x} + \mathbf{c}_i \delta t, t + \delta t) = f_{i,\alpha}(\mathbf{x}, t) - \Lambda_{ik} [f_{k,\alpha}(\mathbf{x}, t) - f_{k,\alpha}^{\text{eq}}(\mathbf{x}, t)] + \frac{\delta t}{2} [3F_{i,\alpha}(\mathbf{x}, t) - F_{i,\alpha}(\mathbf{x}, t - \delta t)]. \quad (34)$$

Scheme II. $\gamma = 1$. With this choice, we have $\bar{D}_i F_{i,\alpha}(\mathbf{x}, t) = D_i F_{i,\alpha}(\mathbf{x}, t)$, which can be discretized by the following implicit finite-difference scheme:

$$D_i F_{i,\alpha}(\mathbf{x}, t) = \frac{F_{i,\alpha}(\mathbf{x} + \mathbf{c}_i \delta t, t + \delta t) - F_{i,\alpha}(\mathbf{x}, t)}{\delta t}. \quad (35)$$

Substituting the above equation into Eq. (33) and introducing the new variable $\bar{f}_{i,\alpha}(\mathbf{x}, t) = f_{i,\alpha}(\mathbf{x}, t) - \delta t F_{i,\alpha}(\mathbf{x}, t)/2$, we can obtain

$$\bar{f}_{i,\alpha}(\mathbf{x} + \mathbf{c}_i \delta t, t + \delta t) = \bar{f}_{i,\alpha}(\mathbf{x}, t) - \Lambda_{ik} [\bar{f}_{k,\alpha}(\mathbf{x}, t) - f_{k,\alpha}^{\text{eq}}(\mathbf{x}, t)] + \delta t \left(\delta_{ik} - \frac{1}{2} \Lambda_{ik} \right) F_{k,\alpha}(\mathbf{x}, t). \quad (36)$$

In this scheme, the macroscopic variable \bar{u}_α is computed by

$$\bar{u}_\alpha = \sum_i f_{i,\alpha} = \sum_i \bar{f}_{i,\alpha} + \frac{\delta t}{2} \bar{F}_\alpha, \quad (37)$$

while the pressure is still given by Eq. (32), with $f_{i,\alpha}$ replaced by $\bar{f}_{i,\alpha}$.

C. The computational schemes for the velocity gradient, velocity divergence, strain rate tensor, shear stress, and vorticity

Besides the fluid velocity and pressure mentioned above, usually, we also need to consider some other physical variables. For instance, the strain rate tensor (or the symmetric velocity gradient tensor), shear stress, and vorticity (it is related to the antisymmetric velocity gradient tensor) are also important in the study of the non-Newtonian fluid flows and turbulence [56,57], and in the framework of LBM, they have also received increasing attention in the past years [23–27,58]. Actually, the strain rate tensor or shear stress can be derived locally from the projection on the second-order polynomial eigenvectors [38,59,60], which is also employed for the construction of local boundary schemes [61]. In the SRT-LB model, Artoli *et al.* [23] developed a local scheme for the shear stress in which the second-order moment of nonequilibrium distribution function is adopted and applied the scheme to study blood flow in a symmetric bifurcation. Then Krüger *et al.* [24] conducted a theoretical analysis and found that the local scheme for the shear stress has a second-order convergence rate. Chai and Zhao [25] further considered the forcing term effect on the computation of the strain rate tensor and

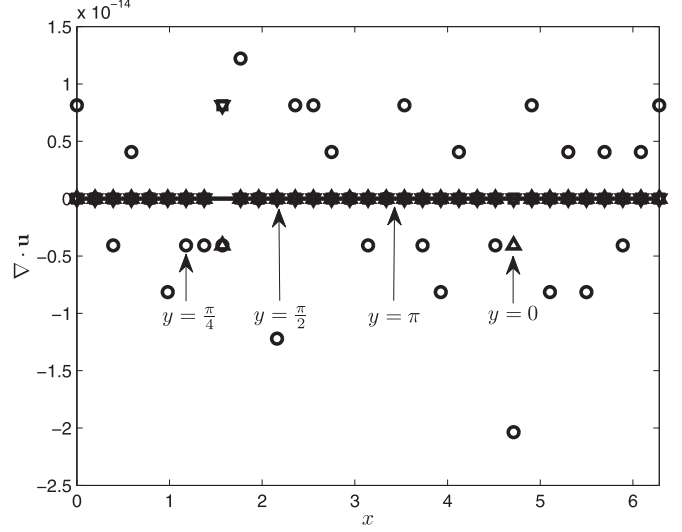


FIG. 10. The numerical and analytical solutions of the velocity divergence at different positions. Solid lines show the analytical solution, and symbols show the numerical solution.

shear stress and proposed two more general local schemes for the strain rate tensor and shear stress. They also performed a theoretical analysis and numerical simulations and demonstrated that the local schemes have second-order accuracy in space. Yong and Luo [26] carried out an asymptotic analysis of the SRT-LB model coupled with the simple bounce-back boundary condition and illustrated that the shear stress computed with the second-order moment of the nonequilibrium distribution function has second-order accuracy in space. In addition, the velocity divergence can also be calculated locally by the second-order moment of the nonequilibrium distribution function [25].

In the LB method, it seems difficult to construct local schemes for the velocity gradient and vorticity, and for this reason, some nonlocal finite-difference schemes are usually adopted (e.g., Ref. [45]). Recently, through the careful design of the high-order moments of the equilibrium distribution function, Peng *et al.* [27] developed a local scheme for the vorticity in the MRT-LB model with D3Q27 lattice structure. However, this scheme cannot be extended to other lattice models, e.g., the commonly used D2Q9 lattice model in two-dimensional space. To overcome this limitation, Hajabdollahi and Premnath [58] proposed another scheme for the computation of vorticity in the double-distribution-function LBM. However, in addition to the LB model for NSEs, they would also need to introduce another LB model for an additional CDE, which would bring greater computational cost. In this work, we will develop a local scheme for the velocity gradient which can be further extended to calculate the velocity divergence, strain rate tensor, shear stress, and vorticity without introducing any additional requirements. Compared to previous works [23–27,58] in which second-order moments of the nonequilibrium distribution function were adopted, the present local schemes for the velocity gradient, velocity divergence, strain rate tensor, shear stress, and vorticity include only the first-order moments of the nonequilibrium distribution function, and what is more, they are not restricted to the special lattice models.

Now let us focus on how to calculate the velocity gradient, velocity divergence, strain rate tensor, shear stress, and vorticity in the MDF-LBM. Actually, from Eq. (27) we can first obtain the velocity gradient,

$$\nabla_{\beta} u_{\alpha} = -\frac{s_1}{\eta c^2 \delta t} \sum_i \mathbf{c}_{i,\beta} f_{i,\alpha}^{ne} \quad (\alpha \neq 0), \quad (38)$$

$$\nabla \cdot \mathbf{u} = \sum_{\alpha=1}^d \nabla_{\alpha} u_{\alpha} = -\frac{s_1}{\eta c^2 \delta t} \sum_{\alpha=1}^d \sum_i \mathbf{c}_{i,\alpha} f_{i,\alpha}^{ne}, \quad (39)$$

$$S_{\alpha\beta} = \frac{1}{2} (\nabla_{\beta} u_{\alpha} + \nabla_{\alpha} u_{\beta}) = -\frac{s_1}{2\eta c^2 \delta t} \sum_i (\mathbf{c}_{i,\beta} f_{i,\alpha}^{ne} + \mathbf{c}_{i,\alpha} f_{i,\beta}^{ne}) \quad (\alpha \neq 0, \beta \neq 0), \quad (40)$$

$$\sigma_{\alpha\beta} = 2\rho_0 v S_{\alpha\beta} = -\rho_0 \left(1 - \frac{s_1}{2}\right) \sum_i (\mathbf{c}_{i,\beta} f_{i,\alpha}^{ne} + \mathbf{c}_{i,\alpha} f_{i,\beta}^{ne}) \quad (\alpha \neq 0, \beta \neq 0), \quad (41)$$

$$\Omega_{\alpha\beta} = \frac{1}{2} (\nabla_{\beta} u_{\alpha} - \nabla_{\alpha} u_{\beta}) = -\frac{s_1}{2\eta c^2 \delta t} \sum_i (\mathbf{c}_{i,\beta} f_{i,\alpha}^{ne} - \mathbf{c}_{i,\alpha} f_{i,\beta}^{ne}) \quad (\alpha \neq 0, \beta \neq 0). \quad (42)$$

Then based on the following relation between the antisymmetric velocity gradient tensor Ω and the vorticity $\omega = \nabla \times \mathbf{u}$,

$$\Omega_{\alpha\beta} = -\frac{1}{2} \epsilon_{\alpha\beta\gamma} \omega_{\gamma}, \quad (43)$$

we can determine the component of vorticity ω_{γ} ; $\epsilon_{\alpha\beta\gamma}$ is the Levi-Civita tensor.

Finally, we also give some remarks on the present MDF-LBM for the convection-diffusion-system-based incompressible NSEs.

Remark 1. In the above analysis, if the diffusive scaling ($\delta t \propto \delta x^2$) is considered [49,63], the evolution equation (3) can be simply written as

$$f_{i,\alpha}(\mathbf{x} + \mathbf{c}_i \delta t, t + \delta t) = f_{i,\alpha}(\mathbf{x}, t) - \mathbf{A}_{ik} [f_{k,\alpha}(\mathbf{x}, t) - f_{k,\alpha}^{\text{eq}}(\mathbf{x}, t)] + \delta t F_{i,\alpha}(\mathbf{x}, t). \quad (44)$$

Then we can also derive the macroscopic equation (28) from Eq. (44), while the truncation error is $O(\delta x^2)$ rather than $O(\delta t^2)$. On the other hand, for the specified kinematic viscosity ν and the relaxation parameter s_1 , we can also obtain the diffusive scaling $\delta t \propto \delta x^2$ from Eq. (29), which means that the diffusive scaling used in the LBM is reasonable. Additionally, the computational schemes for the velocity, pressure, velocity gradient, velocity divergence, strain rate tensor, shear stress, and vorticity are the same as Eqs. (17), (32), (38), (39), (40), (41), and (42). In the following, for simplicity we consider the MDF-LBM (44) for the convection-diffusion-system-based incompressible NSEs.

Remark 2. In the SDF-LBM for the NSEs [23–26], the velocity divergence, strain rate tensor, and shear stress can be computed locally with the second-order moments of the nonequilibrium distribution function, while in the present MDF-LBM for the convection-diffusion-system-based incompressible NSEs, only the first-order moments of the nonequilibrium distribution function are needed, as seen from Eqs. (39), (40), and (41).

Remark 3. In the commonly used LBM for NSEs, it is difficult to compute the velocity gradient locally. However, in

where the truncation error in Eq. (30) has been neglected. We note that Eq. (38) is similar to the schemes reported in previous works [48,62] and can be used to derive the schemes for the velocity divergence $\nabla \cdot \mathbf{u}$, strain rate tensor \mathbf{S} , shear stress σ , and antisymmetric velocity gradient tensor Ω ,

the present MDF-LBM for the convection-diffusion-system-based incompressible NSEs, the velocity gradient can be calculated locally from Eq. (38), which can also be used to determine some other physical variables, including the velocity divergence $\nabla \cdot \mathbf{u}$, strain rate tensor \mathbf{S} , shear stress σ , and vorticity ω . Additionally, we also note that although some local schemes have been developed for the vorticity, there are still some limitations in the available works [27,58]. For example, the local scheme proposed by Peng *et al.* [27] is suitable only for the D3Q27 lattice model and cannot be extended to some other lattice models. Compared to the scheme in Ref. [27], the scheme developed by Hajabdollahi and Premnath [58] is more general, while an additional CDE must be introduced and solved by another LB model, which would make the computational cost more expensive.

Remark 4. In the SDF-LBM for the NSEs [22], the pressure is related to density through the relation $P = \rho \eta c^2$, where the density is calculated with the zeroth order of the distribution function, while in the LBM for incompressible NSEs [64], the pressure is determined by the zeroth-order moment of the distribution function without considering the one in the zeroth direction. In the present MDF-LBM, the pressure is computed by the first-order moment of distribution function, but the one with $\alpha = 0$ is not included. In addition, it should be noted that the formula for the pressure [see Eq. (32)] is consistent with the continuity equation (1a), and thus, we do not need to consider the evolution equation (3) with $\alpha = 0$.

IV. NUMERICAL RESULTS AND DISCUSSION

For simplicity, but without loss of generality, we considered only two-dimensional problems in this section and adopt some two-dimensional benchmark problems, including the Poiseuille flow, the simplified four-roll mill problem, and lid-driven cavity flow, to test the developed MDF-LBM. For brevity, we consider only the D2Q5 lattice model in which the collision matrix \mathbf{A} is taken to be

$$\mathbf{A} = \mathbf{M}^{-1} \mathbf{S}_d \mathbf{M}. \quad (45)$$

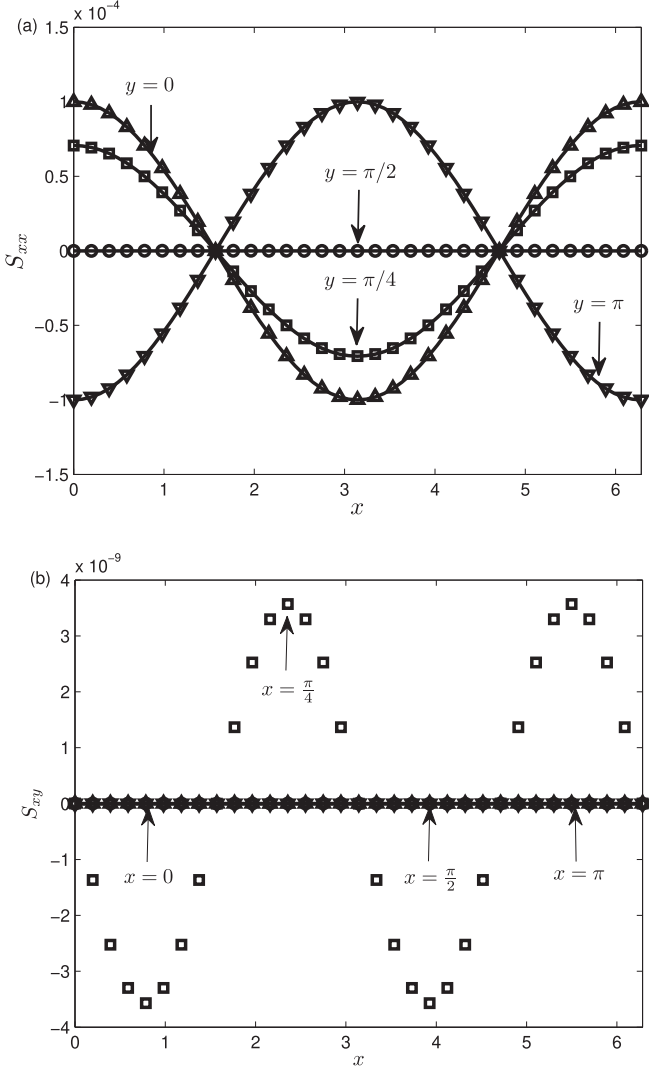


FIG. 11. The numerical and analytical solutions of the components of the strain rate tensor at different positions. (a) S_{xx} and (b) S_{yy} . Solid lines show the analytical solution, and symbols show the numerical solution.

The transformation matrix \mathbf{M} and relaxation matrix \mathbf{S}_d appearing in the above equation are defined as [21]

$$\mathbf{M} = \begin{pmatrix} 1 & 1 & 1 & 1 & 1 \\ 0 & c & 0 & -c & 0 \\ 0 & 0 & c & 0 & -c \\ 0 & c^2 & -c^2 & c^2 & -c^2 \\ -4c^2 & c^2 & c^2 & c^2 & c^2 \end{pmatrix}, \quad (46a)$$

$$\mathbf{S}_d = \mathbf{diag}(s_0, s_1, s_1, s_2, s_2), \quad (46b)$$

where s_i is the relaxation parameter corresponding to the i th-order moment of the distribution function. In this case, the evolution equation (3) will be the same as that in the classical TRT model [31] under the condition $s_0 = s_2$, and the matrix construction in the MRT model can be avoided. Additionally, according to Eq. (8), the relations among the weight coefficients and lattice speed in the D2Q5 lattice model

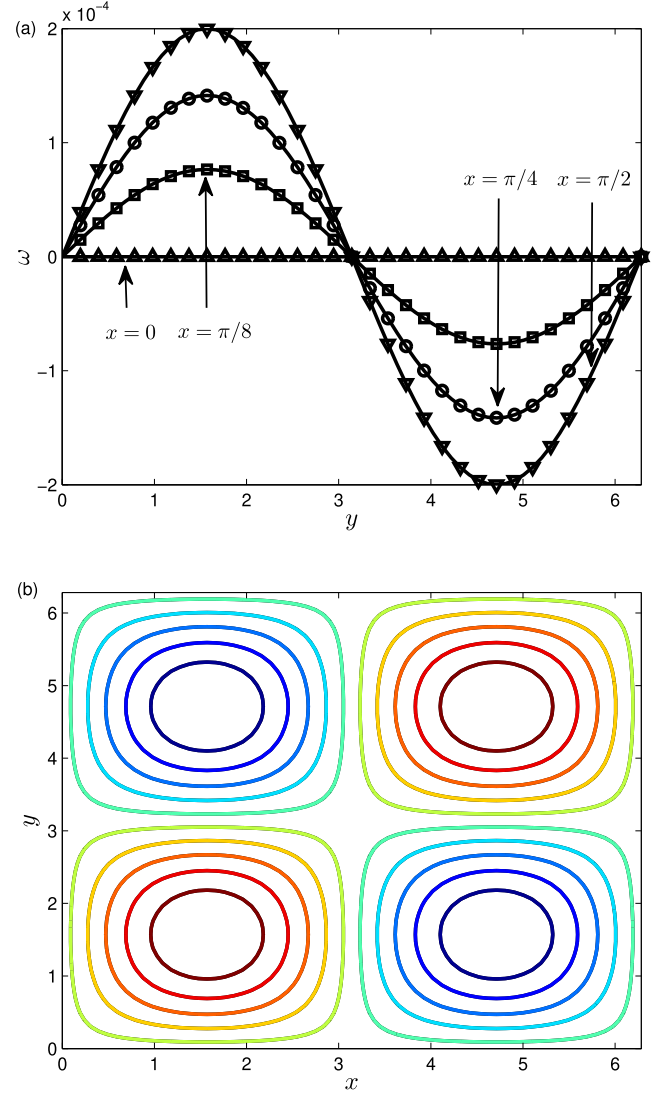


FIG. 12. (a) The numerical and analytical solutions of the vorticity at different positions. Solid lines show the analytical solution, and symbols show the numerical solution. (b) The contour lines of vorticity. The black line shows the analytical solution, and colored lines show the numerical solution.

can be generally expressed as

$$\omega_i = \frac{1 - \omega_0}{4}, \quad 2\omega_i = \eta, \quad i = 1 - 4, \quad (47)$$

where ω_0 is considered a free parameter within the range $(0, 1)$. Actually, if $\omega_0 = 1/5$, we can obtain $\omega_i = 1/5$ ($i = 1 - 4$) and $\eta = 2/5$. However, if $\omega_0 = 1/3$, we have $\omega_i = 1/6$ ($i = 1 - 4$) and $\eta = 1/3$, which is the same as in Eq. (12b) and will be used in the following simulations. It should be noted that some other lattice models can also be adopted in the MRT-LBM for CDE, and the details can be found in some available literature [8]. Unless otherwise stated, the initialization of the distribution functions is realized by their equilibrium distribution functions, where the pressure and velocity are given by $P = 1$ and $u_1 = u_2 = 0$. The halfway anti-bounce-back scheme for the MDF-LBM [17] is used to treat Dirichlet boundary conditions of velocity.

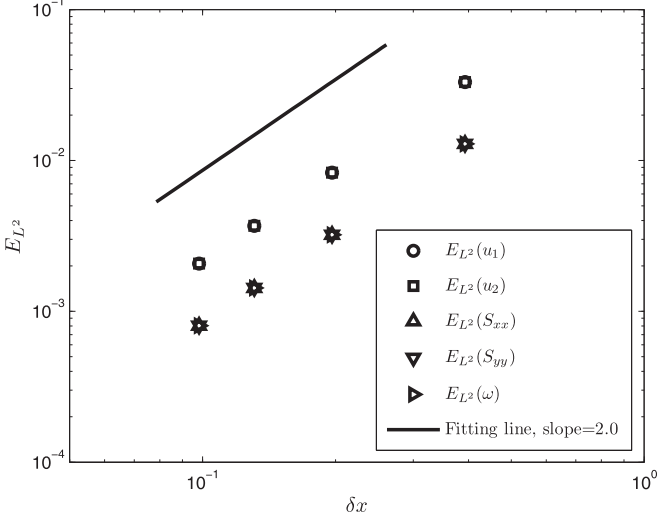


FIG. 13. The convergence rates of the MDF-LBM and the local schemes for the strain rate tensor and vorticity.

In our simulations, to test the accuracies of the MDF-LBM and the local schemes for the physical variables, the following L^2 norm of the relative error E_{L^2} is adopted:

$$E_{L^2}(\phi) = \frac{\|\phi_a(x, y) - \phi_n(x, y)\|_2}{\|\phi_a(x, y)\|_2}, \quad (48)$$

where ϕ denotes the velocity, velocity gradient, velocity divergence, strain rate tensor, or vorticity and the subscripts a and n represent the analytical and numerical solutions of ϕ .

A. The two-dimensional Poiseuille flow

The first problem we considered is the simple Poiseuille flow, which is driven by an external constant force in the x direction ($F_1 = 1.0 \times 10^{-6}$), as shown in Fig. 1. For this problem, we can obtain its analytical solutions for the velocity $\mathbf{u} = (u_1, u_2)^T$, velocity gradient $\nabla \mathbf{u}$, velocity divergence $\nabla \cdot \mathbf{u}$, strain rate tensor \mathbf{S} , and vorticity ω :

$$u_1 = \frac{F_1}{2\nu} H^2 \left[\frac{y}{H} - \left(\frac{y}{H} \right)^2 \right], \quad u_2 = 0, \quad (49a)$$

$$\frac{\partial u_1}{\partial x} = \frac{\partial u_2}{\partial x} = \frac{\partial u_2}{\partial y} = 0, \quad \frac{\partial u_1}{\partial y} = \frac{F_1}{2\nu} H \left(1 - 2 \frac{y}{H} \right), \quad (49b)$$

$$\nabla \cdot \mathbf{u} = \frac{\partial u_1}{\partial x} + \frac{\partial u_2}{\partial y} = 0, \quad (49c)$$

$$S_{xx} = S_{yy} = 0, \quad S_{xy} = S_{yx} = \frac{F_1}{4\nu} H \left(1 - 2 \frac{y}{H} \right), \quad (49d)$$

$$\omega = \frac{\partial u_2}{\partial x} - \frac{\partial u_1}{\partial y} = -\frac{F_1}{2\nu} H \left(1 - 2 \frac{y}{H} \right). \quad (49e)$$

We performed some simulations with the present MDF-LBM, and a lattice size of 32×32 is adopted for the computational domain $[0, 1] \times [0, 1]$ with the periodic boundary condition in the x direction. We present some numerical results in Figs. 2–6, where the kinematic viscosity is $\nu = 0.001$ and the relaxation parameters are set to $s_0 = 1$, $s_1 = 1.2$, and $s_2 = 8(2 - s_1)/(8 - s_1)$ [21,39,42,65]. As shown in Figs. 2–6, the numerical results for the velocity \mathbf{u} , the components of the velocity gradient ($\partial u_1/\partial x$ and $\partial u_1/\partial y$),

TABLE III. The relative errors of the velocity, strain rate tensor, and vorticity under different values of relaxation parameter s_1 .

| | $s_1 = 0.7$ | $s_1 = 1.2$ | $s_1 = 1.7$ |
|-------------------|-------------------------|-------------------------|-------------------------|
| $E_{L^2}(u_1)$ | 3.9869×10^{-3} | 2.0745×10^{-3} | 1.2871×10^{-3} |
| $E_{L^2}(u_2)$ | 3.9869×10^{-3} | 2.0745×10^{-3} | 1.2871×10^{-3} |
| $E_{L^2}(S_{xx})$ | 8.0330×10^{-4} | 8.0328×10^{-4} | 8.0327×10^{-4} |
| $E_{L^2}(S_{yy})$ | 8.0330×10^{-4} | 8.0328×10^{-4} | 8.0327×10^{-4} |
| $E_{L^2}(\omega)$ | 8.0333×10^{-4} | 8.0330×10^{-4} | 8.0330×10^{-4} |

the velocity divergence $\nabla \cdot \mathbf{u}$, the components of the strain rate tensor (S_{xx} and S_{xy}), and the vorticity ω are in good agreement with analytical solutions. In addition, we also measured the relative errors of the velocity u_1 , the component of the velocity gradient $\partial u_1/\partial y$, the component of the strain rate tensor S_{xy} , and the vorticity ω and found that their values are about $E_{L^2}(u_1) = 5.9427 \times 10^{-4}$, $E_{L^2}(\partial u_1/\partial y) = 9.7541 \times 10^{-17}$, $E_{L^2}(S_{xy}) = 9.7541 \times 10^{-17}$, and $E_{L^2}(\omega) = 9.7541 \times 10^{-17}$. It should be noted that the component of the velocity gradient $\partial u_1/\partial y$, the component of the strain rate tensor S_{xy} , and the vorticity ω can achieve machine precision. This is because the local schemes (38), (40), and (42) have second-order accuracy, while the distributions of these physical variables are only linear. In addition, it is also observed from Fig. 4 that the continuity equation $\nabla \cdot \mathbf{u} = 0$ is preserved automatically.

Finally, to examine the Galilean invariance of the present MDF-LBM, we also conducted a numerical test for this problem and present a comparison between the MDF-LBM and SDF-LBM with the following finite-difference scheme for the velocity gradient (strain rate tensor and vorticity) in Table I,

$$\nabla_{\beta} u_{\alpha}(\mathbf{x}) = \sum_{i \neq 0} \frac{\omega_i \mathbf{c}_{i,\beta} u_{\alpha}(\mathbf{x} + \mathbf{c}_{i,\beta} \delta t)}{\eta c^2 \delta t} \quad (\alpha \neq 0, \beta \neq 0), \quad (50)$$

$$S_{\alpha\beta} = \frac{1}{2} (\nabla_{\beta} u_{\alpha} + \nabla_{\alpha} u_{\beta}), \quad \omega = \frac{\partial u_2}{\partial x} - \frac{\partial u_1}{\partial y}. \quad (51)$$

From Table I, we can observe that under different constant velocities u_0 in the x direction, the Galilean invariance errors of the velocity u_1 from these two methods are the same order, while the MDF-LBM performs better for the strain rate tensor and vorticity. The comparisons of the errors $E_{L^2}(S_{xy})$ and $E_{L^2}(\omega)$ can also indicate the advantage of the local schemes. Additionally, it is also found that the SDF-LBM is more stable than the MDF-LBM for large values of u_0 .

B. The simplified two-dimensional four-roll mill problem

The second example we use to test the present MDF-LBM is the simplified two-dimensional four-roll mill problem. A schematic of the problem is given in Fig. 7, where the four rollers are replaced by a body force to drive fluid flow and the physical domain of the problem is $[0, 2\pi] \times [0, 2\pi]$ with periodic boundary conditions in both the x and y directions. As a benchmark problem, it has also been used to test the accuracy of the LBM [25,66] for the following two reasons. The first is that the problem has analytical solutions for the velocity,

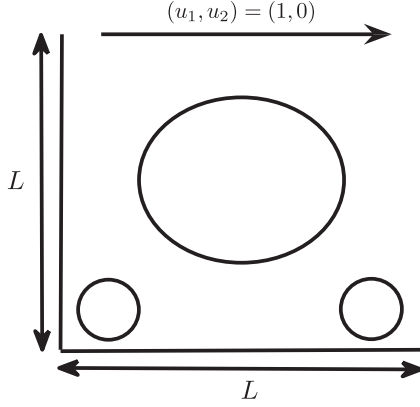


FIG. 14. The schematic of the two-dimensional lid-driven cavity flow.

velocity gradient, velocity divergence, strain rate tensor, and vorticity. The second is that the boundary condition of the problem is periodic such that its effect on the numerical results can be excluded [25]. For the incompressible flow driven by the force

$$F_1 = U_0^2 \sin(x) \cos(x) + 2\nu U_0 \sin(x) \cos(y), \quad (52a)$$

$$F_2 = U_0^2 \sin(y) \cos(y) - 2\nu U_0 \sin(y) \cos(x), \quad (52b)$$

we can obtain analytical solutions for the velocity, velocity gradient, velocity divergence, strain rate tensor, and vorticity,

$$u_1 = U_0 \sin(x) \cos(y), \quad u_2 = -U_0 \cos(x) \sin(y), \quad (53a)$$

$$\frac{\partial u_1}{\partial x} = U_0 \cos(x) \cos(y) = -\frac{\partial u_2}{\partial y}, \quad (53b)$$

$$\frac{\partial u_1}{\partial y} = -U_0 \sin(x) \sin(y) = -\frac{\partial u_2}{\partial x}, \quad (53b)$$

$$\nabla \cdot \mathbf{u} = \frac{\partial u_1}{\partial x} + \frac{\partial u_2}{\partial y} = 0, \quad (53c)$$

$$S_{xx} = U_0 \cos(x) \cos(y) = -S_{yy}, \quad S_{xy} = S_{yx} = 0, \quad (53d)$$

$$\omega = \frac{\partial u_2}{\partial x} - \frac{\partial u_1}{\partial y} = 2U_0 \sin(x) \sin(y). \quad (53e)$$

We carried out some numerical experiments with a lattice size of 64×64 , and the results are shown in Figs. 8–12, where $U_0 = 0.0001$, $\nu = 0.01$, and the relaxation parameters are the same as those used in the first problem. As seen from Figs. 8–12 the numerical results for the velocity, velocity gradient, velocity divergence, strain rate tensor, and vorticity are very close to the corresponding analytical solutions; especially, from the contour lines of the vorticity shown in Fig. 12(b), we can clearly observe that four vortices form at the locations of the rollers.

This problem is also used to test the convergence rates of the present MDF-LBM for velocity and the local schemes for the strain rate tensor and vorticity. To this end, we calculated the relative errors of the velocity, the strain rate tensor, and the vorticity at different lattice sizes ($N \times N = 16 \times 16$, 32×32 , 48×48 , and 64×64) and plot them in Fig. 13. From Fig. 13, we can find that the present MDF-LBM and the local schemes have second-order accuracy in space. To show the performance of the local schemes for the strain rate tensor

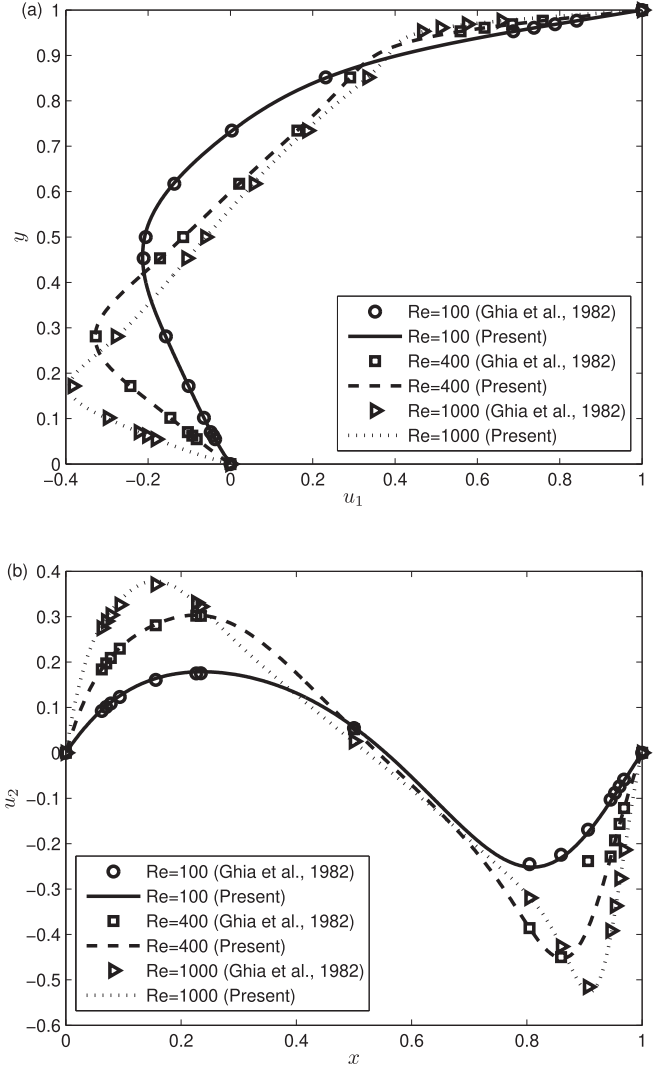


FIG. 15. The profiles of velocity along vertical and horizontal lines through the geometric center of the cavity. (a) u_1 along the vertical line and (b) u_2 along the horizontal line.

and vorticity more clearly, we also conducted a comparison between the local schemes and the nonlocal finite-difference schemes (50) and (51). From the results in Table II, we can observe that the present local schemes are more accurate.

In addition, it is well known that the eigenvalue (or relaxation parameter) s_1 of the collision matrix $\mathbf{\Lambda}$ is a key parameter in the LBM and may also affect the numerical results. Thus, we also conducted some simulations to test the effect of the relaxation parameter s_1 and present the relative errors of the velocity, the strain rate tensor, and the vorticity for three different values of the relaxation parameter s_1 in Table III, where the viscosity and lattice size are fixed to $\nu = 0.01$ and 64×64 . As shown in Table III, the relaxation parameter s_1 has no apparent influence on the numerical results, especially on the strain rate tensor and vorticity.

C. The two-dimensional lid-driven cavity flow

The last problem we considered is the two-dimensional lid-driven cavity flow, and the schematic of the problem is

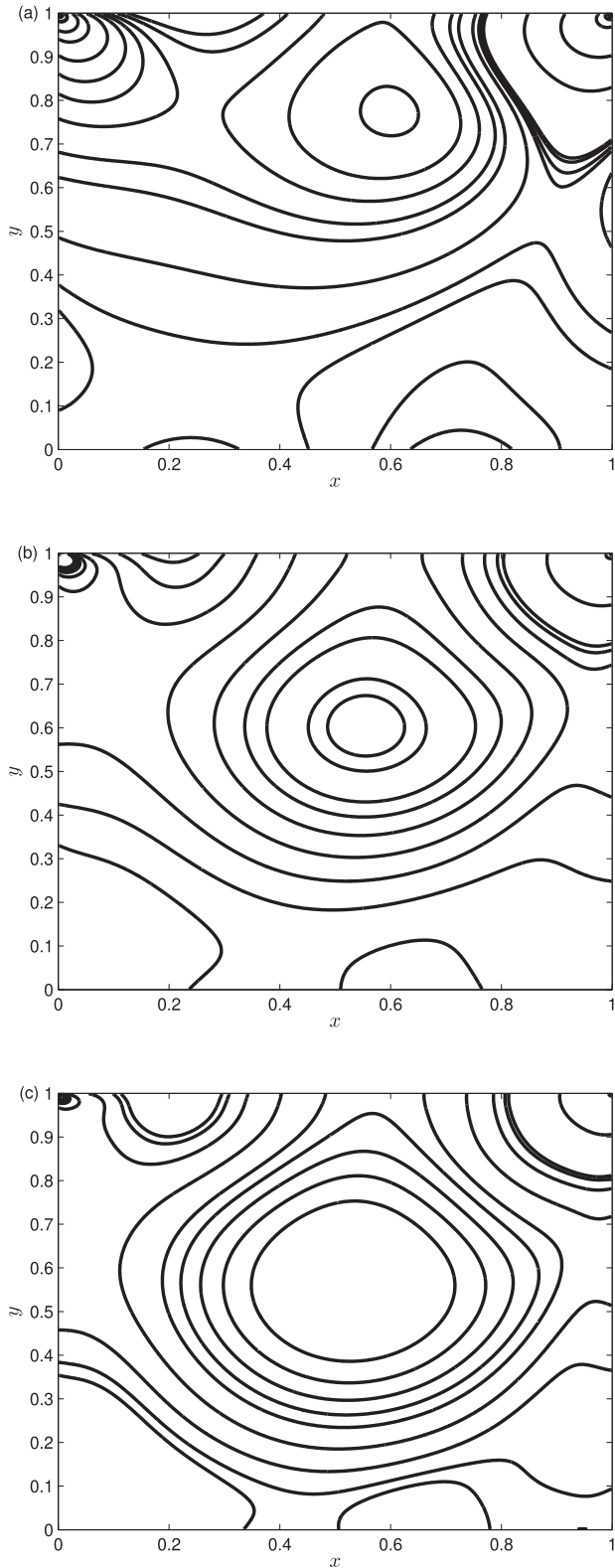


FIG. 16. The contours of pressure at (a) $Re = 100$, (b) 400, and (c) 1000.

shown in Fig. 14, where the length of the square cavity is $L = 1$. Compared to the previous problems, it is more complicated since there is no exact solution available. Although the geometry of the problem is very simple, the lid-driven cavity

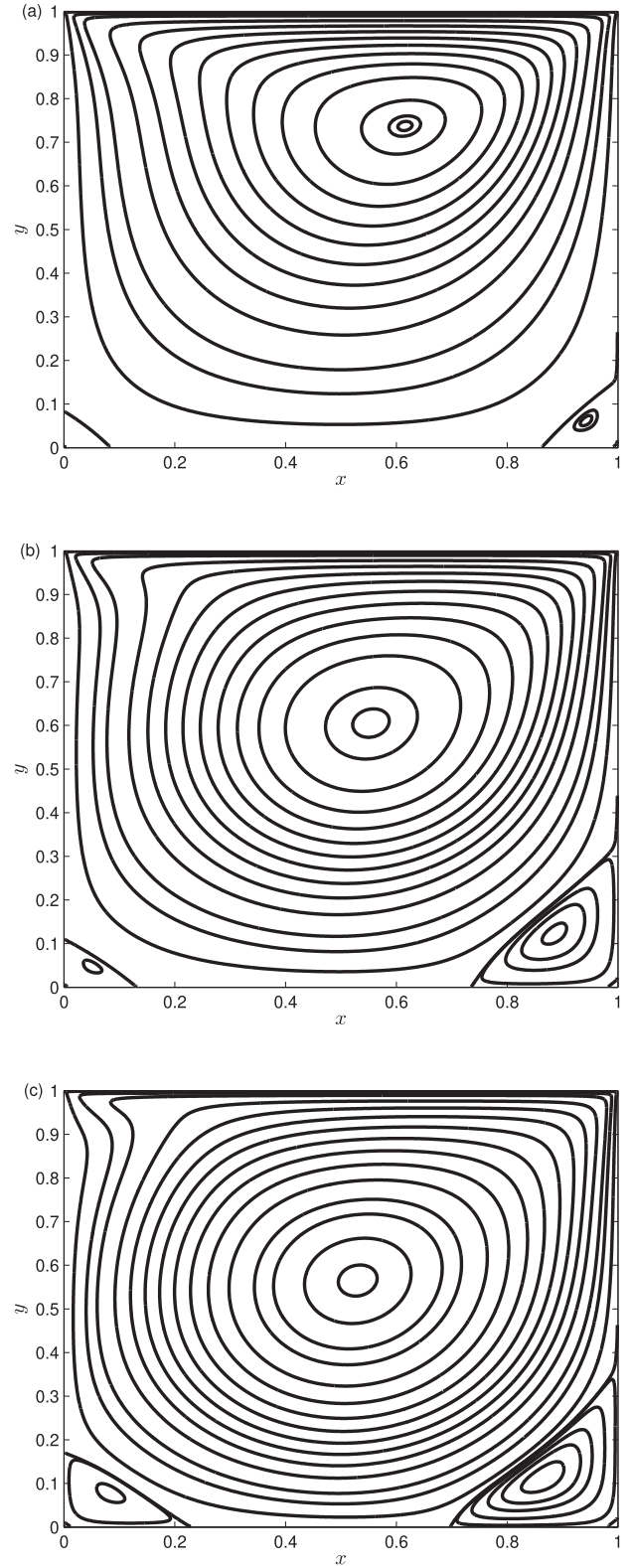


FIG. 17. The streamlines of lid-driven cavity flows at (a) $Re = 100$, (b) 400, and (c) 1000.

flow is of great scientific interest because it displays rich fluid mechanical phenomena, especially complex vortex dynamics [67]. The flow in the square cavity is driven by the top moving wall with a constant velocity, $(U_1, U_2)^T = (1, 0)^T$, and

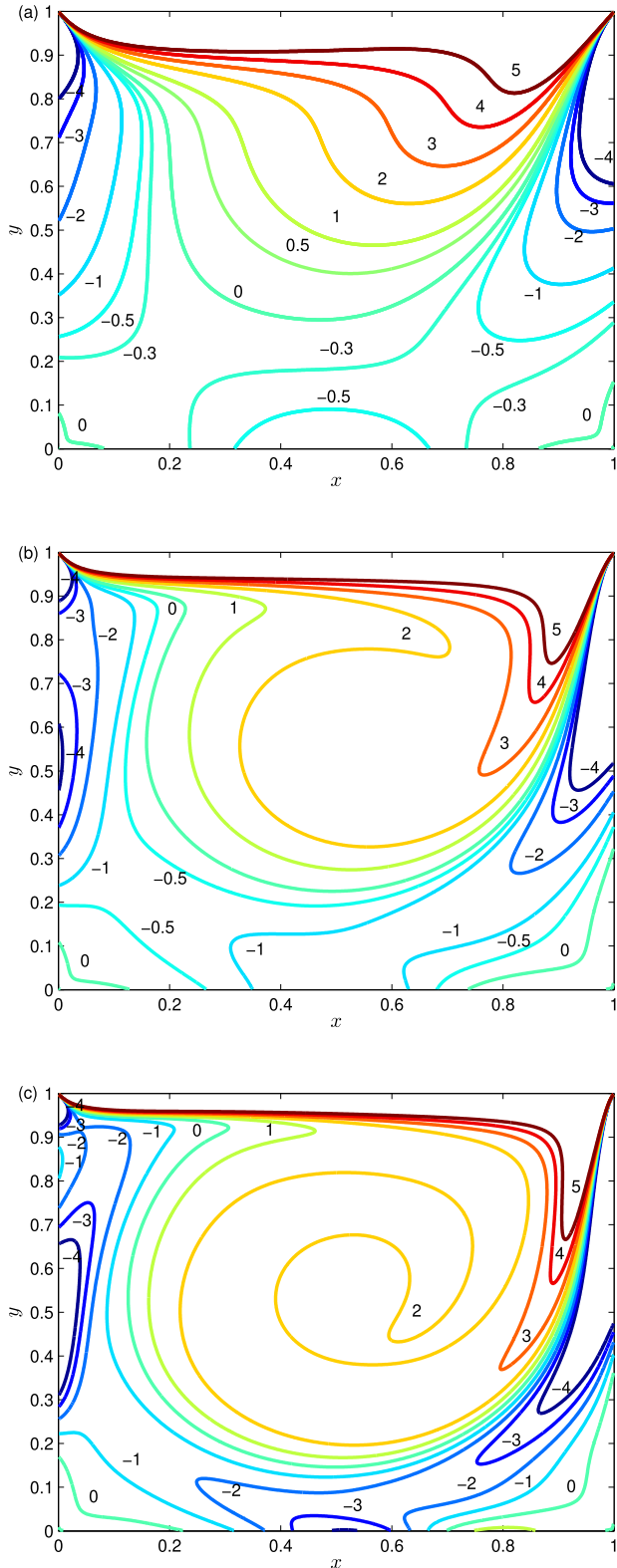


FIG. 18. The contours of the vorticity at (a) $Re = 100$, (b) 400, and (c) 1000.

a primary vortex in the center and some secondary vortices at the corners will form with the increase of the Reynolds number ($Re = LU_1/\nu$). Actually, the lid-driven cavity flow, as a classic benchmark problem, has also been widely used to test the capacity of numerical methods [45,68–71].

TABLE IV. The vorticity ω and location (x, y) of the primary vortex.

| Reference | Parameter | $Re = 100$ | $Re = 400$ | $Re = 1000$ |
|------------|-----------|------------|------------|-------------|
| This study | ω | 3.1655 | 2.2797 | 1.9794 |
| | x | 0.6167 | 0.5540 | 0.5303 |
| | y | 0.7373 | 0.6053 | 0.5651 |
| Ref. [68] | ω | 3.1665 | 2.2947 | 2.0497 |
| | x | 0.6172 | 0.5547 | 0.5313 |
| | y | 0.7344 | 0.6055 | 0.5626 |
| Ref. [69] | ω | 3.1348 | 2.2910 | 2.0760 |
| | x | 0.6196 | 0.5608 | 0.5333 |
| | y | 0.7373 | 0.6078 | 0.5647 |
| Ref. [45] | ω | 3.1629 | 2.2950 | 2.0678 |
| | x | 0.6150 | 0.5546 | 0.5312 |
| | y | 0.7378 | 0.6053 | 0.5663 |

In this part, we conduct some numerical simulations of lid-driven cavity flows at different Reynolds numbers, and to ensure the incompressible condition is valid, the discrete velocity $c = 10$ is adopted to give a small Mach number ($Ma = U_1/\sqrt{\eta}c$). In our simulations, to obtain accurate results, the lattice size is set to be 512×512 , and relaxation parameters are $s_0 = 1$ and $s_2 = 8(2 - s_1)/(8 - s_1)$. We first present the velocity profiles along the vertical and horizontal lines through the geometric center of the cavity in Fig. 15, where $Re = 100, 400, \text{ and } 1000$. As seen from Fig. 15, the

TABLE V. The vorticity ω and location (x, y) of the secondary vortex.

| Vortex | Reference | Parameter | $Re = 100$ | $Re = 400$ | $Re = 1000$ |
|---------------------|------------|-----------|------------|------------|-------------|
| Bottom-left vortex | This study | ω | -0.0149 | -0.0583 | -0.3514 |
| | | x | 0.0343 | 0.0511 | 0.0833 |
| | Ref. [68] | ω | -0.0155 | -0.0570 | -0.3618 |
| | | x | 0.0313 | 0.0508 | 0.0859 |
| | Ref. [69] | ω | -0.0391 | 0.0469 | 0.0781 |
| | | x | 0.0392 | 0.0549 | 0.0902 |
| Bottom-right vortex | This study | ω | -0.0352 | -0.4486 | -1.0690 |
| | | x | 0.9425 | 0.8855 | 0.8650 |
| | Ref. [68] | ω | -0.0331 | -0.4335 | -1.1547 |
| | | x | 0.9453 | 0.8906 | 0.8594 |
| | Ref. [69] | ω | 0.0625 | 0.1250 | 0.1094 |
| | | x | 0.9451 | 0.8902 | 0.8667 |
| Bottom-right vortex | Ref. [45] | ω | -0.0348 | -0.4451 | -1.1039 |
| | | x | 0.9425 | 0.8560 | 0.8645 |
| | Ref. [68] | ω | -0.0331 | -0.4335 | -1.1547 |
| | | x | 0.9453 | 0.8906 | 0.8594 |
| | Ref. [69] | ω | 0.0625 | 0.1250 | 0.1094 |
| | | x | 0.9451 | 0.8902 | 0.8667 |

TABLE VI. A comparison of efficiencies between the present MDF-LBM and SDF-LBM.

| | Method | |
|------------------|---------|---------|
| | MDF-LBM | SDF-LBM |
| 10 000 steps (s) | 552 | 631 |

numerical results are in good agreement with the available data [68]. In addition, we also plot the distributions of the pressure in Fig. 16 and find that these results qualitatively agree with those in previous works [45,69]. To show the complex dynamics of lid-driven cavity flows, we also plot the streamlines and vorticity contours in Figs. 17 and 18. From Figs. 17 and 18, we can observe that a primary vortex in the center of the cavity and two secondary vortices in two bottom corners form. Simultaneously, it is also found that with the increase of the Reynolds number, the primary vortex moves towards the center of the cavity. To quantify these results, we measured the vorticities and locations of the primary and secondary vortices and list them in Tables IV and V. As shown in Tables IV and V, the present results are very close to those reported in some previous studies [45,68,69].

In addition, to show the efficiency of the present MDF-LBM, we also present a comparison of the computational times in the present MDF-LBM and the SDF-LBM [Eqs. (50) and (51) are used to calculate the strain rate tensor and vorticity] for this problem, and the results are shown in Table VI. From Table VI, we can find that the present MDF-LBM is more efficient, which is attributed to the use of the linear equilibrium distribution function. Actually, most of the computational time in the LBM is used to calculate the equilibrium distribution function.

V. CONCLUSIONS

In this work, a MDF-LBM coupled with the MRT model was developed for incompressible NSEs. To do this, the

NSEs were first reformulated into a convection-diffusion system, and then the MDF-LBM was proposed for the convection-diffusion system. What is more, in addition to the macroscopic pressure and velocity, we also proposed some local schemes for the velocity gradient, velocity divergence, strain rate tensor, shear stress, and vorticity in the framework of the MDF-LBM. To test the capacity of the MDF-LBM and local schemes, three benchmark problems, including the two-dimensional Poiseuille flow, the simplified four-roll mill problem, and the lid-driven cavity flow, were considered. The numerical results show that the present MDF-LBM and local schemes are efficient and also have a second-order convergence rate in space.

It should be noted that compared to the classic LBM for two-dimensional incompressible NSEs for which the D2Q9 lattice model should be used, the MDF-LBM is more flexible since the D2Q4, D2Q5, or D2Q9 lattice model can be adopted to give the correct incompressible NSEs. Additionally, in the MDF-LBM for convection-diffusion-system-based NSEs, some physical variables (e.g., the velocity gradient, the velocity divergence, the strain rate tensor, the shear stress, and the vorticity) can be computed locally through the first-order moments of the nonequilibrium distribution function, while in the commonly used SDF-LBM for incompressible NSEs, usually, only the velocity divergence, the strain rate tensor, and the shear stress can be determined locally by the second-order moments of the nonequilibrium distribution function.

Finally, we would also like to point out that the present MDF-LBM can be extended to study the thermal flows and multiphase fluid system governed by the incompressible NSEs and CDE, which will be considered in another work.

ACKNOWLEDGMENTS

This work was financially supported by the National Natural Science Foundation of China (Grants No. 12072127 and No. 51836003), and the computation was completed on the HPC Platform of Huazhong University of Science and Technology.

-
- [1] R. Benzi, S. Succi, and M. Vergassola, The lattice Boltzmann equation: Theory and applications, *Phys. Rep.* **222**, 145 (1992).
 - [2] S. Chen and G. Doolen, Lattice Boltzmann method for fluid flows, *Annu. Rev. Fluid Mech.* **30**, 329 (1998).
 - [3] C. K. Aidun and J. R. Clausen, Lattice-Boltzmann method for complex flows, *Annu. Rev. Fluid Mech.* **42**, 439 (2010).
 - [4] A. Xu, W. Shyy, and T. Zhao, Lattice Boltzmann modeling of transport phenomena in fuel cells and flow batteries, *Acta Mech. Sin.* **33**, 555 (2017).
 - [5] H. Wang, X. Yuan, H. Liang, Z. Chai, and B. Shi, A brief review of the phase-field-based lattice Boltzmann method for multiphase flows, *Capillarity* **2**, 33 (2019).
 - [6] D. A. Wolf-Gladrow, *Lattice-Gas Cellular Automata and Lattice Boltzmann Models: An Introduction* (Springer, Berlin, 2000).
 - [7] S. Succi, *The Lattice Boltzmann Equation for Fluid Dynamics and Beyond* (Oxford University Press, Oxford, 2001).
 - [8] Z. Guo and C. Shu, *Lattice Boltzmann Method and Its Applications in Engineering* (World Scientific, Singapore, 2013).
 - [9] H. Huang, M. C. Sukop, and X.-Y. Lu, *Multiphase lattice Boltzmann methods: Theory and applications* (Wiley, Chichester, 2016).
 - [10] T. Krüger, H. Kusumaatmaja, A. Kuzmin, O. Shardt, G. Silva, and E. M. Viggien, *The Lattice Boltzmann Method: Principles and Practice* (Springer, Cham, 2017).
 - [11] F. Bouchut, Construction of BGK models with a family of kinetic entropies for a given system of conservation laws, *J. Stat. Phys.* **95**, 113 (1999).
 - [12] M. F. Carfora and R. Natalini, A discrete kinetic approximation for the incompressible Navier-Stokes equations, *ESAIM: Math. Modell. Numer. Anal.* **42**, 93 (2008).
 - [13] R. Bianchini and R. Natalini, Convergence of a vector-BGK approximation for the incompressible Navier-Stokes equations, *Kinet. Relat. Models* **12**, 133 (2019).

- [14] F. Dubois, Simulation of strong nonlinear waves with vectorial lattice Boltzmann schemes, *Int. J. Mod. Phys. C* **25**, 1441014 (2014).
- [15] J. Zhao, Discrete-velocity vector-BGK models based numerical methods for the incompressible Navier-Stokes equations, *Commun. Comput. Phys.* **29**, 420 (2020).
- [16] J. Zhao and Z. Zhang, Seven-velocity three-dimensional vectorial lattice Boltzmann method including various types of approximations to the pressure and two-parameterized second-order boundary treatments, *Comput. Math. Appl.* **80**, 2764 (2020).
- [17] J. Zhao, Z. Zhang, and W.-A. Yong, Vector-type boundary schemes for the lattice Boltzmann method based on vector-BGK models, *SIAM J. Sci. Comput.* **42**, B1250 (2020).
- [18] X. Shan, Simulation of Rayleigh-Bénard convection using a lattice Boltzmann method, *Phys. Rev. E* **55**, 2780 (1997).
- [19] X. He, S. Chen, and G. D. Doolen, A novel thermal model for the lattice Boltzmann method in incompressible limit, *J. Comput. Phys.* **146**, 282 (1998).
- [20] Z. Guo, B. Shi, and C. Zheng, A coupled lattice BGK model for the Boussinesq equations, *Int. J. Numer. Methods Fluids* **39**, 325 (2002).
- [21] S. Cui, N. Hong, B. Shi, and Z. Chai, Discrete effect on the halfway bounce-back boundary condition of multiple-relaxation-time lattice Boltzmann model for convection-diffusion equations, *Phys. Rev. E* **93**, 043311 (2016).
- [22] Y. H. Qian, D. d’Humières, and P. Lallemand, Lattice BGK models for Navier-Stokes equation, *Europhys. Lett.* **17**, 479 (1992).
- [23] A. M. Artoli, D. Kandhai, H. C. J. Hoefsloot, A. G. Hoekstra, and P. M. A. Sloop, Lattice BGK simulations of flow in a symmetric bifurcation, *Future Gener. Comput. Syst.* **20**, 909 (2004).
- [24] T. Krüger, F. Varnik, and D. Raabe, Shear stress in lattice Boltzmann simulations, *Phys. Rev. E* **79**, 046704 (2009).
- [25] Z. Chai and T. S. Zhao, Effect of the forcing term in the multiple-relaxation-time lattice Boltzmann equation on the shear stress or the strain rate tensor, *Phys. Rev. E* **86**, 016705 (2012).
- [26] W.-A. Yong and L.-S. Luo, Accuracy of the viscous stress in the lattice Boltzmann equation with simple boundary conditions, *Phys. Rev. E* **86**, 065701(R) (2012).
- [27] C. Peng, Z. Guo, and L.-P. Wang, Lattice Boltzmann model capable of mesoscopic vorticity computation, *Phys. Rev. E* **96**, 053304 (2017).
- [28] L. D. Landau and E. M. Lifshitz, *Fluid Mechanics*, 2nd ed. (Pergamon Press, Oxford, 1987).
- [29] P. K. Kundu, I. M. Cohen, and D. Dowling, *Fluid Mechanics* (Elsevier, San Diego, 2016).
- [30] H. Chen, S. Chen, and W. H. Matthaeus, Recovery of the Navier-Stokes equations using a lattice-gas Boltzmann method, *Phys. Rev. A* **45**, R5339 (1992).
- [31] I. Ginzburg, Equilibrium-type and link-type lattice Boltzmann models for generic advection and anisotropic-dispersion equation, *Adv. Water Resour.* **28**, 1171 (2005).
- [32] I. Ginzburg, F. Verhaeghe, and D. d’Humières, Two-relaxation-time lattice Boltzmann scheme: About parametrization, velocity, pressure and mixed boundary conditions, *Commun. Comput. Phys.* **3**, 427 (2008).
- [33] D. d’Humières, Generalized lattice-Boltzmann equations, in *Rarefied Gas Dynamics: Theory and Simulations*, edited by B. D. Shizgal and D. P. Weave, Progress in Astronautics and Aeronautics Vol. 159 (AIAA Press, Washington, DC, 1992), pp. 450–458.
- [34] P. Lallemand and L.-S. Luo, Theory of the lattice Boltzmann method: Dispersion, dissipation, isotropy, Galilean invariance, and stability, *Phys. Rev. E* **61**, 6546 (2000).
- [35] Z. Chai and B. Shi, Multiple-relaxation-time lattice Boltzmann method for the Navier-Stokes and nonlinear convection-diffusion equations: Modeling, analysis, and elements, *Phys. Rev. E* **102**, 023306 (2020).
- [36] I. Ginzburg and D. d’Humières, Multireflection boundary conditions for lattice Boltzmann models, *Phys. Rev. E* **68**, 066614 (2003).
- [37] C. Pan, L.-S. Luo, and C. T. Miller, An evaluation of lattice Boltzmann schemes for porous medium flow simulation, *Comput. Fluids* **35**, 898 (2006).
- [38] S. Khirevich, I. Ginzburg, and U. Tallarek, Coarse-and fine-grid numerical behavior of MRT/TRT lattice-Boltzmann schemes in regular and random sphere packings, *J. Comput. Phys.* **281**, 708 (2015).
- [39] I. Ginzburg, Generic boundary conditions for lattice Boltzmann models and their application to advection and anisotropic dispersion equations, *Adv. Water Resour.* **28**, 1196 (2005).
- [40] T. Zhang, B. Shi, Z. Guo, Z. Chai, and J. Lu, General bounce-back scheme for concentration boundary condition in the lattice-Boltzmann method, *Phys. Rev. E* **85**, 016701 (2012).
- [41] Z. Chai, B. Shi, and Z. Guo, A multiple-relaxation-time lattice Boltzmann model for general nonlinear anisotropic convection-diffusion equations, *J. Sci. Comput.* **69**, 355 (2016).
- [42] I. Ginzburg, Steady-state two-relaxation-time lattice Boltzmann formulation for transport and flow, closed with the compact multi-reflection boundary and interface-conjugate schemes, *J. Comput. Sci.* **54**, 101215 (2021).
- [43] Z. Chai, C. Huang, B. Shi, and Z. Guo, A comparative study on the lattice Boltzmann models for predicting effective diffusivity of porous media, *Int. J. Heat Mass Transfer* **98**, 687 (2016).
- [44] I. Ginzburg, Prediction of the moments in advection-diffusion lattice Boltzmann method. II. Attenuation of the boundary layers via double- Λ bounce-back flux scheme, *Phys. Rev. E* **95**, 013305 (2017).
- [45] L.-S. Luo, W. Liao, X. Chen, Y. Peng, and W. Zhang, Numerics of the lattice Boltzmann method: Effects of collision models on the lattice Boltzmann simulations, *Phys. Rev. E* **83**, 056710 (2011).
- [46] I. Rasin, S. Succi, and W. Miller, A multi-relaxation lattice kinetic method for passive scalar diffusion, *J. Comput. Phys.* **206**, 453 (2005).
- [47] H. Yoshida and M. Nagaoka, Multiple-relaxation-time lattice Boltzmann model for the convection and anisotropic diffusion equation, *J. Comput. Phys.* **229**, 7774 (2010).
- [48] Z. Chai and T. S. Zhao, Nonequilibrium scheme for computing the flux of the convection-diffusion equation in the framework of the lattice Boltzmann method, *Phys. Rev. E* **90**, 013305 (2014).
- [49] M. Zhang, W. Zhao, and P. Lin, Lattice Boltzmann method for general convection-diffusion equations: MRT model and boundary schemes, *J. Comput. Phys.* **389**, 147 (2019).

- [50] B. Chopard, J. L. Falcone, and J. Latt, The lattice Boltzmann advection-diffusion model revisited, *Eur. Phys. J.: Spec. Top.* **171**, 245 (2009).
- [51] S. Chapman and T. G. Cowling, *The Mathematical Theory of Non-uniform Gases* (Cambridge University Press, Cambridge, 1970).
- [52] W.-A. Yong, W. Zhao, and L.-S. Luo, Theory of the lattice Boltzmann method: Derivation of macroscopic equations via the Maxwell iteration, *Phys. Rev. E* **93**, 033310 (2016).
- [53] A. Wagner, Thermodynamic consistency of liquid-gas lattice Boltzmann simulations, *Phys. Rev. E* **74**, 056703 (2006).
- [54] F. Dubois, Equivalent partial differential equations of a lattice Boltzmann scheme, *Comput. Math. Appl.* **55**, 1441 (2008).
- [55] D. d’Humières and I. Ginzburg, Viscosity independent numerical errors for Lattice Boltzmann models: From recurrence equations to “magic” collision numbers, *Comput. Math. Appl.* **58**, 823 (2009).
- [56] R. B. Bird, R. C. Armstrong, and O. Hassager, *Dynamics of Polymeric Liquids*, Fluid Mechanics (Wiley, New York, 1987), Vol. 1.
- [57] W. D. McComb, *The Physics of Fluid Turbulence* (Clarendon Press, Oxford, 1990).
- [58] F. Hajabdollahi and K. N. Premnath, Local vorticity computation approach in double distribution functions based lattice Boltzmann methods for flow and scalar transport, *Int. J. Heat Fluid Flow* **83**, 108577 (2020).
- [59] U. Frisch, D. d’Humières, B. Hasslacher, P. Lallemand, Y. Pomeau, and J.-P. Rivet, Lattice gas hydrodynamics in two and three dimensions, *Complex Syst.* **1**, 649 (1987).
- [60] I. Ginzburg and K. Steiner, Lattice Boltzmann model for free-surface flow and its application to filling process in casting, *J. Comput. Phys.* **185**, 61 (2003).
- [61] I. Ginzbourg and D. d’Humières, Local second-order boundary method for lattice Boltzmann models, *J. Stat. Phys.* **84**, 927 (1996).
- [62] Z. Chai and T. S. Zhao, Lattice Boltzmann model for the convection-diffusion equation, *Phys. Rev. E* **87**, 063309 (2013).
- [63] M. Junk, A. Klar, and L.-S. Luo, Asymptotic analysis of the lattice Boltzmann equation, *J. Comput. Phys.* **210**, 676 (2005).
- [64] Z. Guo, B. Shi, and N. Wang, Lattice BGK model for incompressible Navier-Stokes equation, *J. Comput. Phys.* **165**, 288 (2000).
- [65] Y. Wu, Y. Zhao, Z. Chai, and B. Shi, Discrete effects on some boundary schemes of multiple-relaxation-time lattice Boltzmann model for convection-diffusion equations, *Comput. Math. Appl.* **80**, 531 (2020).
- [66] O. Malaspinas, N. Fiétier, and M. Deville, Lattice Boltzmann method for the simulation of viscoelastic fluid flows, *J. Non-Newtonian Fluid Mech.* **165**, 1637 (2010).
- [67] P. N. Shankar and M. D. Deshpande, Fluid Mechanics in the driven cavity, *Annu. Rev. Fluid Mech.* **32**, 93 (2000).
- [68] U. Ghia, K. N. Ghia, and C. T. Shin, High-Re solutions for incompressible flow using the Navier-Stokes equations and a multigrid method, *J. Comput. Phys.* **48**, 387 (1982).
- [69] S. Hou, Q. Zou, S. Chen, and G. Doolen, Simulation of cavity flow by the lattice Boltzmann method, *J. Comput. Phys.* **118**, 329 (1995).
- [70] O. Botella and R. Peyret, Benchmark spectral results on the lid-driven cavity flow, *Comput. Fluids* **27**, 421 (1998).
- [71] E. Erturk and C. Gökçöl, Fourth-order compact formulation of Navier-Stokes equations and driven cavity flow at high Reynolds number, *Int. J. Numer. Methods Fluids* **50**, 421 (2006).